EXPERIMENTAL STUDY OF THE DEVELOPMENT OF PLASTIC SOLITARY WAVES IN ONE-DIMENSIONAL GRANULAR MEDIA

BY

TOMMY ON

THESIS

Submitted in partial fulfillment of the requirements
for the degree of Master of Science in Aerospace Engineering
in the Graduate College of the
University of Illinois at Urbana-Champaign, 2011

Urbana, Illinois

Advisor:

Professor John Lambros

Abstract

In this work, a modified split Hopkinson pressure bar (SHPB) is used to impact one-dimensional granular chain of spheres. These homogeneous chains used here comprise of brass, aluminum, or stainless steel spherical beads, ranging from a single sphere to a chain of fourteen, and are of interest because of their unique wave propagation characteristics, as seen in earlier efforts. Loading magnitudes spanning from 9 kN to 40 kN – considerably higher than most previous works on these systems which have been conducted in the elastic regime – cause the granular chains to deform plastically. These conditions allow for solitary waves, which propagate in the one-dimensional array of elastic spheres, to be studied in the plastic regime. The propagating pulse assumes a distinctive shape after travelling through five beads, and can consequently be realized as a plastic solitary wave. The wave speed of this pulse was seen to depend on maximum force, as in the elastic as, although it was measured to be less than the elastic wave speed. In addition, the plastic velocity varied with the $1/9^{th}$ power instead of the $1/6^{th}$ power for the elastic speed. For the case of brass, the plastic wave propagates at 50% to 80% the speed of the elastic wave, depending on whether the incident or transmitted force is compared. It was found that there is also decreasing plasticity along the chain length except at the end beads in contact with the SHPB, which rebounds into the bar and are hit again. This research is the first to investigate in detail the development and evolution of a plastic solitary wave and will form the basis of future work in this area.

Acknowledgements

The author would like to express his utmost appreciation to Professor John Lambros for his assistance and guidance for the past two years. In addition, special thanks to Erheng Wang for his helpful contributions, Jodi Gritten for ordering research materials, and the machinists who manufactured parts needed to conduct the experiments: Greg Milner and Dustin Burns. Special thanks to the US Army Research Office under the MURI grant W911NF- 09-1-0436 and the program monitor Dr. David Stepp. Finally, thanks to my family for their support.

Table of Contents

Chapter 1

Introduction

1.1 Background and Motivation

Granular materials such as sand, gravel, sugar, and rice are everywhere in daily life. A granular medium can flow like a liquid, can be transported by the wind, and can be strong enough to support buildings. This variety of behavior has sparked interest in the research of these materials both from the fluid mechanics and the solid mechanics point of view. Granular media can transfer loads differently than continuum materials and support different types of propagating waves, such as a solitary wave. This phenomenon has been extensively studied in recent years. However, most of the studies conducted are in the elastic regime.

The goal of this research is to determine the existence and nature of solitary waves in plastically deforming granular media. Here, by granular media we refer to an arrangement of macroscopic particles in mechanical contact. In the simplest form of an idealized granular medium, these particles can be considered spherical in shape. A one-dimensional array of these particles will be referred to as a "granular chain". Solitary waves occur in granular chains under dynamic loading, and have been examined both numerically and experimentally in elastic chains (*e.g.*, Sen *et al.,* 2008). However, little work has been performed in the plastic regime of grain deformation. In the plastic regime two nonlinear responses act simultaneously: (i) the nonlinear contact between neighboring grains (responsible for the solitary wave generation in the elastic case), and (ii) the material nonlinearity introduced by plasticity. How these two interact is currently an open question. The interplay between these two nonlinear phenomena is studied in

this research to gain a better understanding of plastic solitary waves, and allow possible control and tunability of such waves for desirable results in microstructural material tailoring.

1.1.1 *Properties of Spherical Contact*

The contact between two elastic spheres is commonly modeled as the Hertz contact problem (Hertz, 1882). This considers two bodies contacting together, creating a resultant force between them over the small region of the surface of each body where the contact exists. A detailed formulation of the Hertz contact between spheres has been performed by Johnson (1985). This Hertzian formulation uses the following three assumptions: (1) the radii of curvature of the contacting bodies are large compared to the size of the contact region, allowing each surface to be treated as an elastic half-space, (2) the dimensions of each body are large compared with the radius of the contact region allowing the indentation stresses and strains to be independent from the evolving geometry, and (3) the contact is frictionless. These assumptions result in the contact between two elastic spheres behaving nonlinearly, and in fact without any linear component, while under compression. In addition the contact can, clearly, not sustain any tensile load. Due to these geometrical contact effects, the elastic force F_o exerted on two identical spheres in contact is related the distance of approach d of their centers by

$$d = \frac{2(\theta F_o)^{2/3}}{a^{1/3}}, \qquad \text{with} \quad \theta \equiv \frac{3(1-\upsilon^2)}{4E}, \tag{1.1}$$

where a is the sphere radius, E is the Young's modulus, and υ is the Poisson's ratio. When δ, the distance between the center of two spheres, becomes greater than $2a$, no force is exerted, as shown schematically in Figure 1.1a (δ is taken to be positive in compression). It is clear from Figure 1.1a that the nonlinearity of this (elastic) contact law at the origin is intrinsic, meaning

that there is no elastic content in it whatsoever. Figure 1.1b shows a visual representation of δ and d.

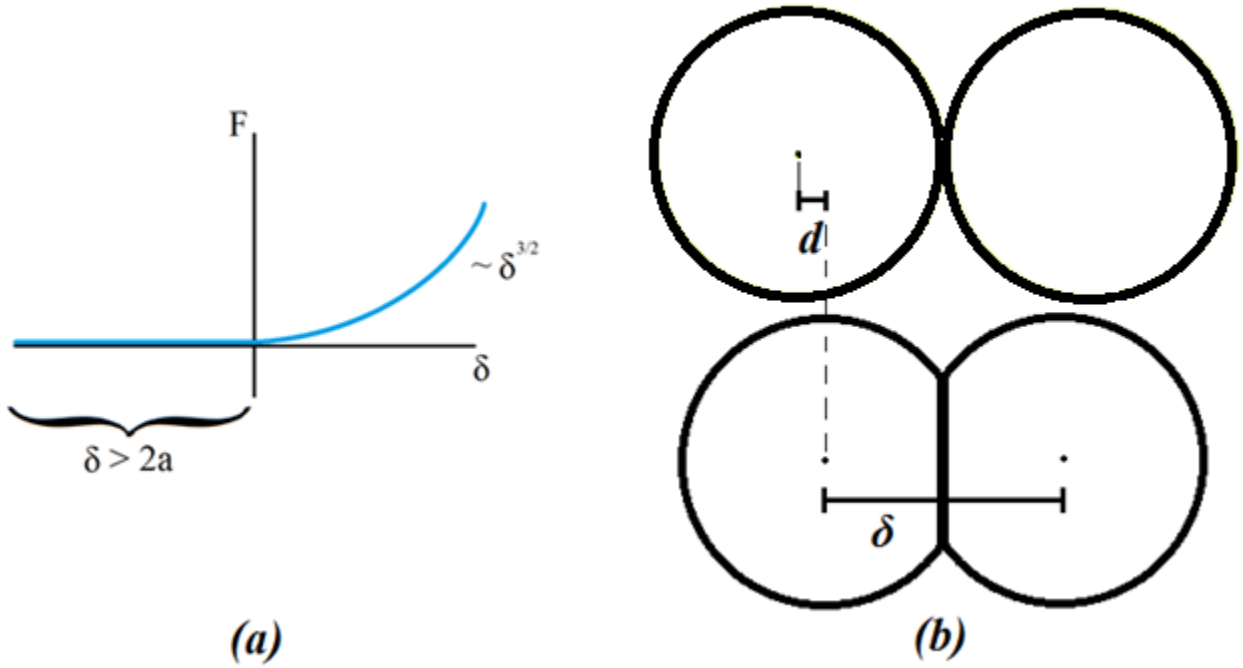

Figure 1.1. (a) Nonlinear contact relation between two spheres. (b) Diagram of two spheres before and during compression.

1.1.2 *Differences Between Granular Media and Continuous Media*

In many cases granular media may appear to behave similarly to a bulk material as a whole, but recent detailed studies conducted show some significant differences. Such a difference is the stress "allocation" in granular media. Some researchers (*e.g.*, Kanatani, 1979; Chang and Ma, 1991) argue that the stress tensor in granular media is not symmetric, and local couple stresses are critical to understanding the behavior of such media. However, Christoffersen *et al.,* (1981) claim that the stress asymmetry is negligible and complicates the description of the mechanical behavior of granular media. Of course, as is well known, the general stress tensor in

a bulk medium is symmetric. Figure 1.2, taken from Bardet and Vardoulakis (2001), helps illustrate the differences between these two types of media configurations. The figure shows the transmission of force from the boundary, where loads are applied, to the interior of the material for a granular medium (left) and a continuum (right). The small triangles show contact locations among different grains, which are therefore able to transfer the external forces along some directions better than others, forming what are usually referred to as force chains (Cates *et al.,* 1998; Bouchaud *et al.,* 2001). In the granular medium, the orientation and magnitude of the stresses depends on each grain coupling, and can be different from another couple.

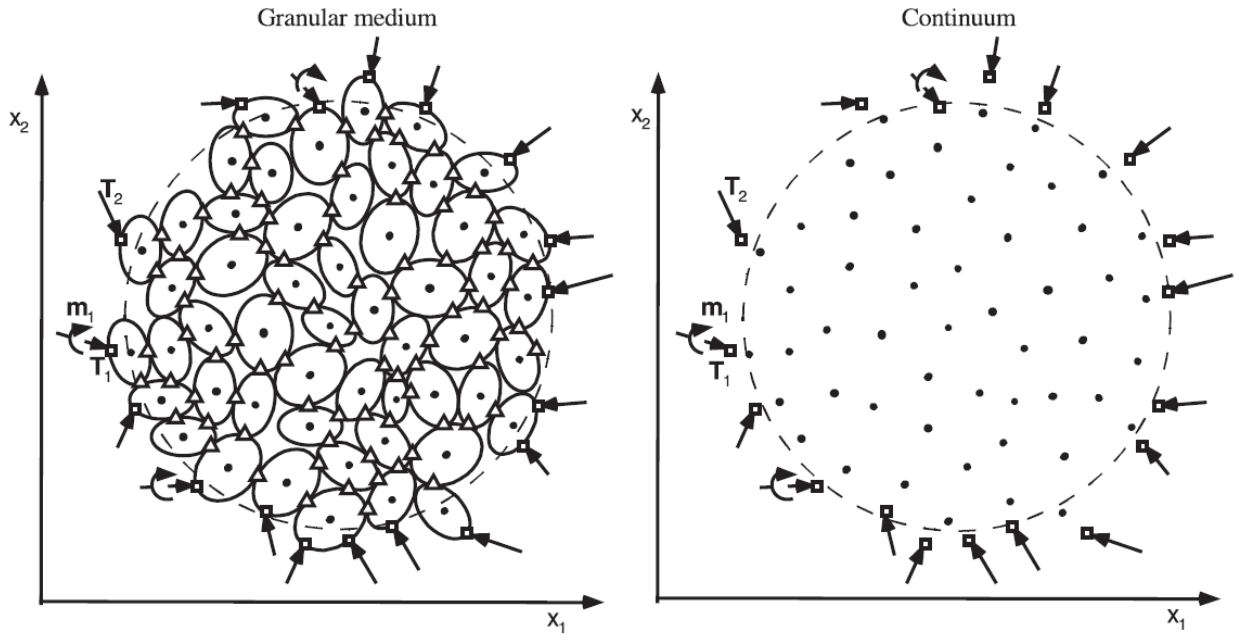

Figure 1.2. Visual differences between granular and continuum medium (taken from Bardet and Vardoulakis, 2001).

When the granular particles are arranged in a one-dimensional array, or chain, they still exhibit a different behavior from a continuous medium. While this configuration allows the stress waves to propagate along a line through it, a chain of spheres will generate nonlinear stress

wave propagation due to the Hertzian contact discussed earlier. As a consequence of the interaction law shown in Figure 1.1a, which exhibits a sonic vacuum since it is not linearizable even for small magnitudes of force, only a solitary wave will be generated in the granular chain. A solitary wave has certain characteristics different than regular stress waves in a continuum: (1) the solitary wave maintains its shape as it propagates through the chain, (2) the wave propagates with a width of approximately five particle diameters in the chain, and (3) the speed of the wave is a function of the maximum input force, material properties of the particle, and the size of the particle, as illustrated in Figure 1.3. The velocity of propagating waves in the one-dimensional system scales as $F_{max}^{1/6}$ (Iida 1938, 1939; Coste *et al.* 1995). However, this relation does not seem to be verified for higher dimensions due to geometrical effects explained by Goddard (1990). To better understand the wave propagation phenomena in plastic granular media, the experiments conducted here will all be on one-dimensional granular chains.

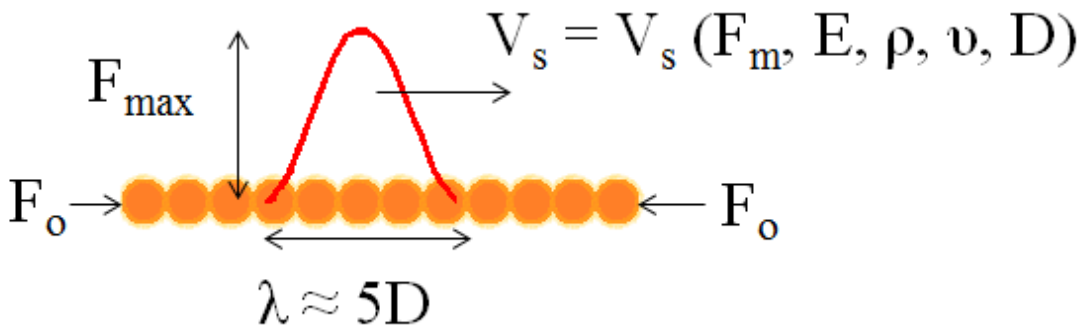

Figure 1.3. Schematic of a solitary wave in a granular chain.

1.2 Solitary Wave in an Elastic Chain

While studying the nonlinear behavior of a chain of beads, Nesterenko (1984) gave an analytical solution to the problem for Hertz's contact law. Nesterenko (1983) has shown that the

dynamic response of granular media can support linear, weakly nonlinear and strongly nonlinear regimes for wave propagation. When the input load is in the same amplitude range as the static compressive force F_o (see Figure 1.3 for definition of F_o), the weakly nonlinear regime is achieved. In this regime, the propagating stress wave is oscillatory, and does not show signs of a solitary wave. This is partially caused by the magnitude of the precompression, which causes the chain to be relatively denser, allowing oscillating waves to transfer between the beads. When the input load is much greater than the static force acting on the chain, the strongly nonlinear regime is reached. Unlike harmonic waves in linear elastic media, a chain of granular media can support propagation of nonlinear solitary waves in the strongly nonlinear regime. Experimental evidence of these solitary waves in the strongly nonlinear regime was conducted by Lazaridi and Nesterenko (1985). A solitary wave in this regime propagates with a speed V_s and with a force magnitude much higher than F_o. This velocity is dependent on the maximum force F_m and particle properties such as the Young's modulus E, bulk density ρ, Poisson's ratio v, and bead diameter a. The exact solution for this solitary wave, which contains the shape of a cos^4 function, has a finite length equal to five particle diameters for a Hertzian contact interaction. In the strongly nonlinear regime, the speed of the solitary wave V_s derived by Daraio *et al.* (2006), reduces to

$$V_s = 0.6802 \left(\frac{2E}{a\rho^{\frac{3}{2}}(1-\nu^2)} \right)^{1/3} F_m^{1/6}. \tag{1.2}$$

Further studies on the dynamic behavior of granular media have been conducted by Shukla (1990; 1991; 1992) by using photoelasticity to study wave propagation in granular chains made of polymeric disks, assumed to behave elastically in these experiments. The wavelength of

the loading pulse used was several times greater than the particle size. This condition allows the loading around the contact regions to be assumed as quasi-static in nature. Thus, Hertz's contact law can be used to obtain the stresses, strains, and loads at each contact point. It was found that at a given contact, the load from the propagating wave increased from zero to a peak value, and then gradually decreased to zero. The peak loads decreased by 20 percent as the wave traveled through five disk diameters, which is considerably higher than the two percent drop observed in a bar of uniform material over the same distance. Though the forces involved allowed the disks to remain elastic, the difference in force reduction shows move variability in the granular case than in a continuum medium. Additional experiments conducted by Coste *et al.* (1997) on 51 stainless steel bead chains observed pulses that propagate over a great distance, with a constant velocity and shape, matching signs of a solitary wave. Their bead chains were loaded via a vibration exciter with a maximum force of 100 N, and the results were in fair agreement with the theoretical predictions of Nesterenko (1983). The relatively small magnitude of the input force used (100 N) allowed the 51 stainless steel beads to remain elastic during the entire experiment.

1.3 Objectives

The main purpose of this experimental investigation is to provide a better understanding on the propagation of solitary waves in granular media when material nonlinearity, in the form of plasticity, is involved. Because of the high stresses at the contact region, yielding is expected to occur even under fairly small loads, and will become dominant as load levels increase. In fact, it can be shown that the load necessary to produce yielding in the spherical contact of two identical spheres of an elastic-perfectly plastic material of elastic modulus E and yield strength σ_y is

$$\frac{P_y}{E^* R^{*2}} = \frac{\pi^3}{6}\left(1.6\frac{\sigma_y}{E^*}\right)^3, \quad \text{with} \quad R^* = \frac{a}{2} \quad \text{and} \quad E^* = \frac{E}{2(1-\nu^2)}, \tag{1.3}$$

where P_y is the force for the yielding, a is the sphere radius and ν is the Poisson's ratio (Johnson, 1985). Most experiments conducted so far in the literature to investigate solitary waves have gone to great lengths to use impact loads small enough not to introduce significant plasticity. However, in any practical applications of these materials, loads will be considerably higher. For example for typical properties for aluminum sphere contact of the size of particles used here P_y is only 1.6 N. Therefore there is knowledge gap in the understanding of how material and contact nonlinearities interact, whether solitary waves exist, and if they do, whether they possess the same characteristics as the elastic solitary waves. Therefore the specific objectives of this work are:

- To study the formation of a solitary wave in the plastic regime on a one-dimensional granular chain, including whether a solitary wave exists in the plastic case, and if it does, how many contacting particles are necessary for it to develop;
- To compare the propagating wave velocity as a function of the maximum input force in the elastic and plastic case;
- To find a correlation between the plastic propagating wave and the magnitude of the irreversible plastic deformation that occurs within a chain of beads.

1.4 Outline

This thesis reports research conducted on the testing of various sets of granular chains to achieve the objectives listed above. Chapter 2 describes the experimental tools used to generate plastic loading in one-dimensional granular chains, extract data from the granular media, and

how the data is analyzed. Chapter 3 discusses the continuum dynamic stress-strain response of the same materials used in the granular chain experiments. This will yield the, possibly rate dependent, material nonlinearity inherent in the beads. The contact nonlinearity in the dynamic regime is studied elsewhere (Wang and Lambros, 2011). Chapter 4 details the behavior of the solitary wave in the plastic chain, the speed of wave propagation in the chain, and physical deformations as a result of the irreversible plasticity, and chapter 5 provides conclusions drawn from this experimental effort.

Chapter 2

Experimental Techniques Based on the Split Hopkinson Pressure Bar

2.1 The Split Hopkinson Pressure Bar (SHPB)

The SHPB, also known as the Kolsky bar, is a characterization tool which experimentally measures the mechanical response of materials deformed at high strain rates (10^2/s to 10^4/s). Since materials may behave differently when loaded statically and dynamically (here dynamically refers to impact loading), it is desirable to investigate material properties under both conditions. A strong impact, such as a hammer hit, can deform a specimen up to failure, but the details of the loading are not easily known or controllable. To obtain the dynamic material response under well-controlled dynamic loading, Kolsky (1949) devised the SHPB. Instead of using a direct impact of a single bar, as initially used by Hopkinson (1914), two elastic bars were employed, one on each side of the specimen, and an explosive blast was used to load one of the bars. The elastic bar between the impact source and the specimen is called the incident bar, and that after the specimen is called the transmission or transmitted bar, as shown in Figure 2.1.

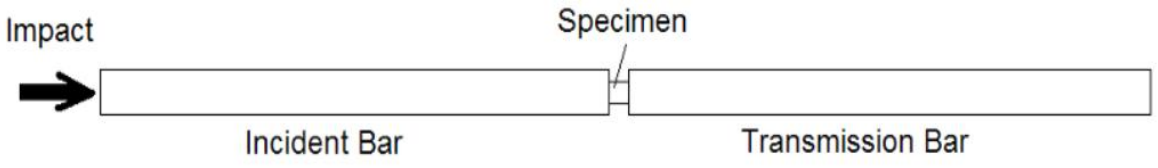

Figure 2.1. Schematic of a split Hopkinson pressure bar.

A modified SHPB is used here to gather the data presented in this thesis. Instead of explosive loading, a light single stage pressurized gas gun fires a projectile onto the incident bar. The projectile used is a shorter elastic rod made from the same material as the incident and transmission bars, and with the same diameter. The incident bar, transmission bar, striker bar, and momentum trap (discussed later) are manufactured from C350 maraging steel, which has a density ρ = 8100 kg/m^3, Young's modulus E = 200 GPa, and bar velocity $c = \sqrt{E/\rho}$ = 4970 m/s. The incident, transmission, and striker bars have a diameter of 12.7 mm and lengths of 3.04 m, 1.83 m, and 0.152 m, respectively. Strain gages are placed half way along the length of the incident and transmitted bars, and on opposite ends to compensate for strain readings caused by possible bending in the bars. Resistor strain gage EA-06-250BK-10C from Vishay Micromeasurements was used for all tests. All strain gages were connected through a signal conditioner which amplified the strain and sent it to an Agilent Technologies Digital Oscilloscope.

2.1.1 *Elastic Wave Theory*

Basic elastic wave propagation theory helps explain the progression of waves in a standard SHPB experiment. When the striker bar is launched from the gas gun and impacts the incident bar, two compressive waves are created at the contact zone, travelling in opposing directions away from the impact. The compressive wave in the striker reaches the free end of the shorter striker first and reflects back as a tensile wave which unloads the striker bar/incident bar interface and removes the contact between them, thus causing the compressive wave travelling in the incident bar to also unload. This compressive pulse of finite size propagates along the incident bar until it reaches the specimen, where an impedance mismatch occurs and causes both a reflected and transmitted pulse. The interface between the specimen and transmission bar also

causes another impedance mismatch and another two additional waves. The final transmitted wave propagates through the transmission bar and reflects back from its free end. This evolution of waves is visualized in Figure 2.2 which displays an *x-t* plot of the waves in the SHPB. The red lines denote a compressive wave and the blue lines represent a tensile wave. The green lines denote the reflections within the specimen. The stresses within a specimen require approximately four reflections to reach homogenization (Ravichandran and Subhash, 1994). The areas shaded in grey are regions where stress is present and the white areas are regions of quiescence.

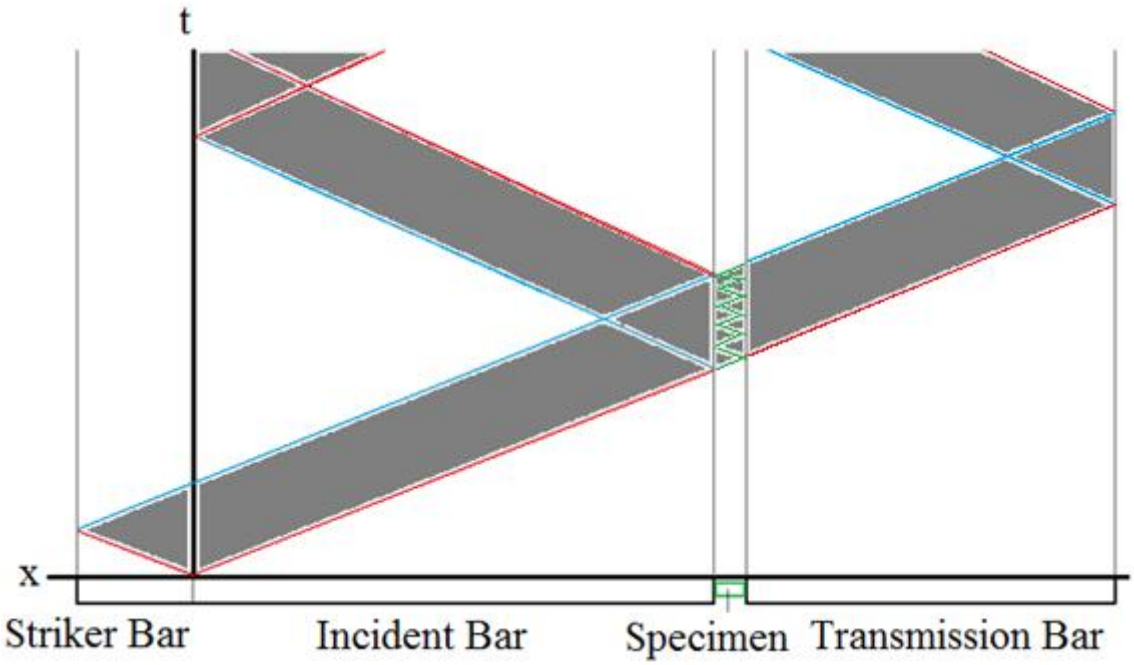

Figure 2.2. X-t plot of waves travelling in a SHPB.

When testing cylindrical samples (as is traditionally done) and stress homogenization in the sample is reached, the following equations are satisfied:

$$F_{in} = A_b E(\varepsilon_I + \varepsilon_R), \tag{2.1}$$

$$F_{out} = A_b E(\varepsilon_T), \tag{2.2}$$

$$F_{out} = F_{in} \quad \Rightarrow \quad \varepsilon_T = \varepsilon_I + \varepsilon_R, \tag{2.3}$$

where F_{in} and F_{out} correspond to the input and output force into the sample, A_b is the cross-sectional area of the bar, and ε_I, ε_R, and ε_T are the strain of the incident, reflected, and transmitted signal, respectively. Using one-dimensional wave propagation assumptions, the engineering stress and strain as a function of time in the sample can be calculated according to (Nemat-Nasser, 2000):

$$\sigma_e(t) = \frac{A_b E \varepsilon_T(t)}{A_s}, \tag{2.4}$$

$$\varepsilon_e(t) = \int_0^t \dot{\varepsilon}_e\,(t) = \int_0^t \frac{2c\varepsilon_R(\tau)}{l_o}\, d\tau, \tag{2.5}$$

where σ_e is the engineering stress in the sample, A_s is the initial cross-sectional area of the sample, c is the speed of sound of the material, l_o is the initial length of the sample, and ε_e is the engineering strain. By knowing the stresses as a function of time, the velocities of the specimen-bar interfaces can be calculated from (Kolsky, 1949)

$$\dot{u}_1 = \dot{u}_I + \dot{u}_R = -\frac{\sigma_I}{\rho c} + \frac{\sigma_R}{\rho c} \quad \text{and} \quad \dot{u}_2 = \dot{u}_T = -\frac{\sigma_T}{\rho c} \tag{2.6}$$

where $\dot{u}_1$ is the velocity of the incident bar and specimen interface, $\dot{u}_2$ is the velocity of the transmitted bar and specimen interface, and the subscripts *I, R, T* are the corresponding velocity and stresses for the incident, reflected, and transmitted signals. The displacements of the two

specimen-bar interfaces can be calculated by integrating the velocities, which are a function of time, over the duration of the pulses.

2.1.2 *Controllable Loading Rates and Profiles*

The SHPB generally loads the specimen between the strain rates of 10^2/s to 10^4/s with a trapezoidal loading pulse, as shown in the incident signal termed "no shaper" in Figure 2.3. This type of input generates a large range of frequencies, and does not necessarily produce a constant rate of deformation in the specimen. The pressure in the gun can be varied, but that alone cannot span differences in two orders of magnitudes for the loading rate, and cannot change the shape of the pulse. Therefore, an additional need for pulse shaping techniques exists so that (a) a larger range of rates can be produced, and (b) specimen homogenization time (*i.e.*, the time after which $F_{in}=F_{out}$) can be prolonged (Ravichandran and Subhash, 1994; Li and Lambros, 1999). A pulse shaper can consist of any material which is added to the beginning of the incident bar to alter the incident pulse profile. Christensen *et al.* (1972) were among the first researchers to use a pulse shaping technique to improve the accuracy of loading a specimen with a near constant rate compressive pulse. For extracting material properties, such as a dynamic stress-strain curve, a constant loading rate would increase the accuracy of the results. Several incident pulses that we have achieved in our experimental set-up with the addition of pulse shaping are shown in Figure 2.3. This figure clearly shows the large difference in the oscillations within a pulse with and without shaping. Also seen in Figure 2.3 is the duration of the incident pulses, which all lie in a similar range. The duration of such a pulse is controlled by the duration of loading. In the case of this setup, the loading is from the impact of the bullet; hence the duration of the loading pulse depends on the length of the bullet as explained earlier. However, pulse shapers can also affect the input duration, as for example the case of a ductile Cu layer in Figure 2.3.

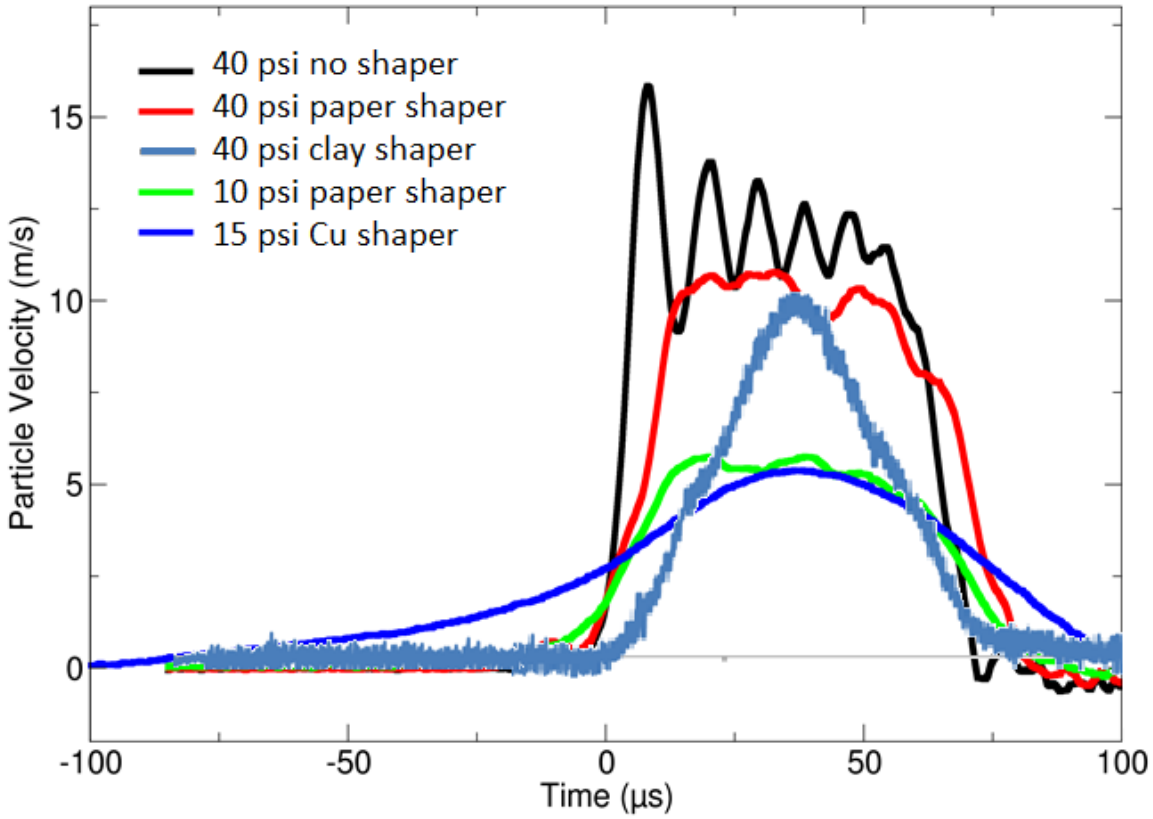

Figure 2.3. Incident signals with and without a pulse shaper (with contributions from Jamie Kimberly).

When the bullet or striker bar impacts the incident bar, the stress wave generated propagates back and forth within the SHPB system. Usually, only the pulses associated with the first loading wave are recorded, but the subsequent reflections are still able to induce multiple loading cycles onto the specimen. This can cause invalidated postmortem analyses of the specimen since the data recorded will be for the first loading, but the sample observed in any postmortem microscopy would have undergone multiple loadings. The concept of stopping additional stress waves from reaching the specimen, commonly known as momentum trapping,

first appeared in the early 1960s by Baker and Yew (1966). A later rendition of the momentum trap was developed by Nemat-Nasser *et al.* (1991) and is shown schematically in Figure 2.4. In addition to the conventional SHPB design, a transfer flange, an incident tube covering the bar, and a reaction mass are used. The incident tube is placed in contact with the transfer flange and reaction mass. When the striker impacts the transfer flange, it creates two compression pulses: one traveling in the incident bar towards the specimen and another traveling in the incident tube towards the reaction mass. The compression wave in the tube is reflected from the reaction mass and travels back to the transfer flange again as compression. This compressive wave is reflected from the traction free flange end as tension causing the incident bar to move in the reverse direction and avoiding additional compression of the specimen. We have implemented such a device in our SHPB and all experiments shown here have used the momentum trap, unless otherwise noted. A typical incident pulse generated with this arrangement contains a compression followed immediately by a tension which unloads the sample, as shown in Figure 2.5 with compression being show as positive.

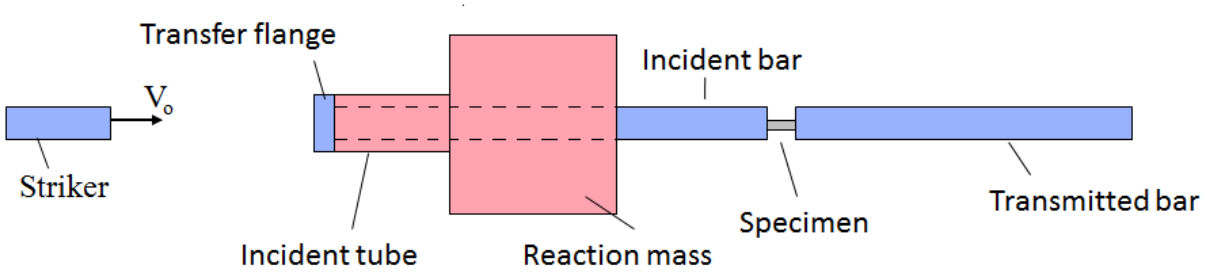

Figure 2.4. Schematic of compression momentum trap.

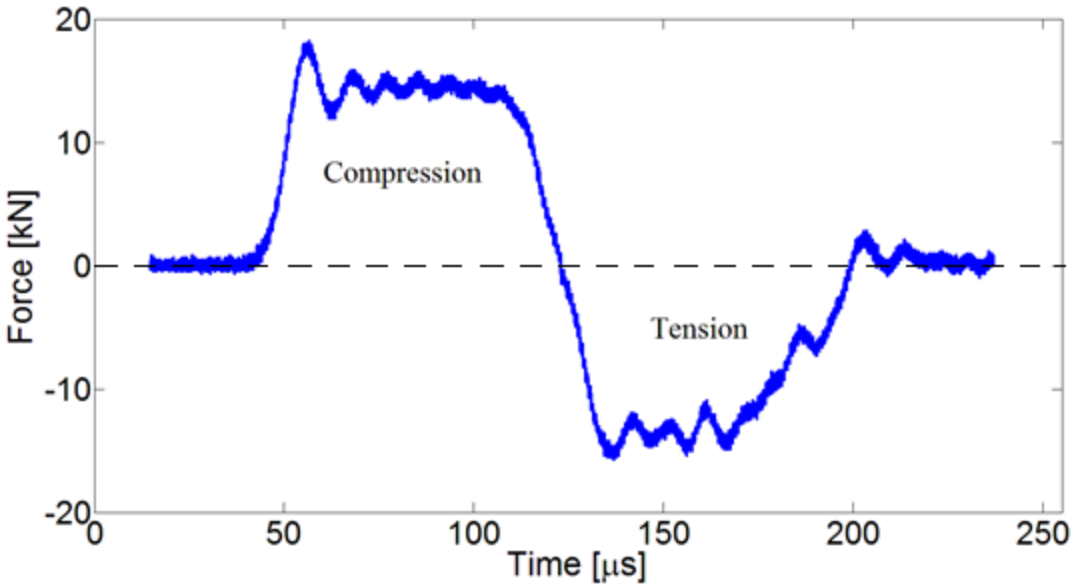

Figure 2.5. Incident signal generated with momentum trap.

The tensile portion of the incident pulse can be generated immediately after the compressive part ends by making the incident tube the same length as the striker bar, if both are comprised of the same material. The momentum trap can act as a loading duration limiter in addition to trapping successive input stress waves. This also limits the duration of the extended pulse caused by the use of pulse shapers. Two incident signals are shown in Figure 2.6, one with a momentum trap and one without. As seen, the differences in these signals are not noticeable, since the momentum trap should not affect the first part of the incident signal. However, the momentum trap does ensure that only a single loading pulse reaches the specimen which allows accurate post mortem measurements. As stated above, the majority of the experiments shown in this thesis are conducted with a momentum trap, unless otherwise noted.

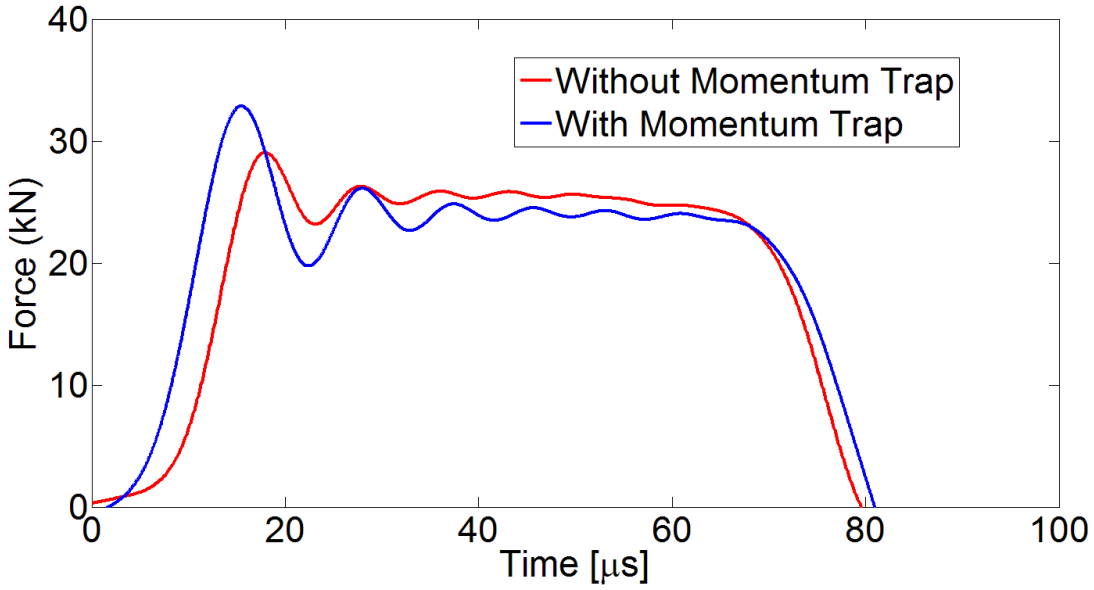

Figure 2.6. Incident signals with and without a momentum trap.

2.2 Adaptation for Testing Granular Chains

As discussed in the introduction, here we are interested in studying the formation of solitary waves in granular chains subjected to high loads and high loading rates. A modification of the SHPB will be used for this purpose. The specimens studied in this thesis are linear arrays of spherical beads consisting of three metallic materials: brass alloy 260, aluminum alloy 2017, and stainless steel alloy 302. All beads are 9.5 mm in diameter, and a test specimen consists of either single beads or one-dimensional homogeneous chains of beads of lengths two to fourteen.

Since the SHPB was mainly designed as a material characterization tool for cylindrical specimens, the same analysis as discussed above cannot be performed on spherical beads which would not necessarily be expected to reach a homogenized state. Without equilibrium in the forces on either side of a specimen, stress data cannot be accurately derived. Also, in some cases the resulting transmitted signal is quite low, so the transmission bar of C350 maraging steel was

replaced with an aluminum 6061 bar of equal length in those cases. Since the recorded data are strain measurements, the aluminum bar will produce higher strain and create a larger signal. This is important when the transmitted signal for an experiment is on the same order as the noise in the signal. Figure 2.7 shows a comparison of two tests conducted on ten-bead brass chains. Both tests had similar incident pulses, but the signal of the transmitted bar in the C350 maraging steel bar is comparable to the noise. This problem is alleviated by using the more compliant aluminum bar. The aluminum bar remains elastic throughout the experiments.

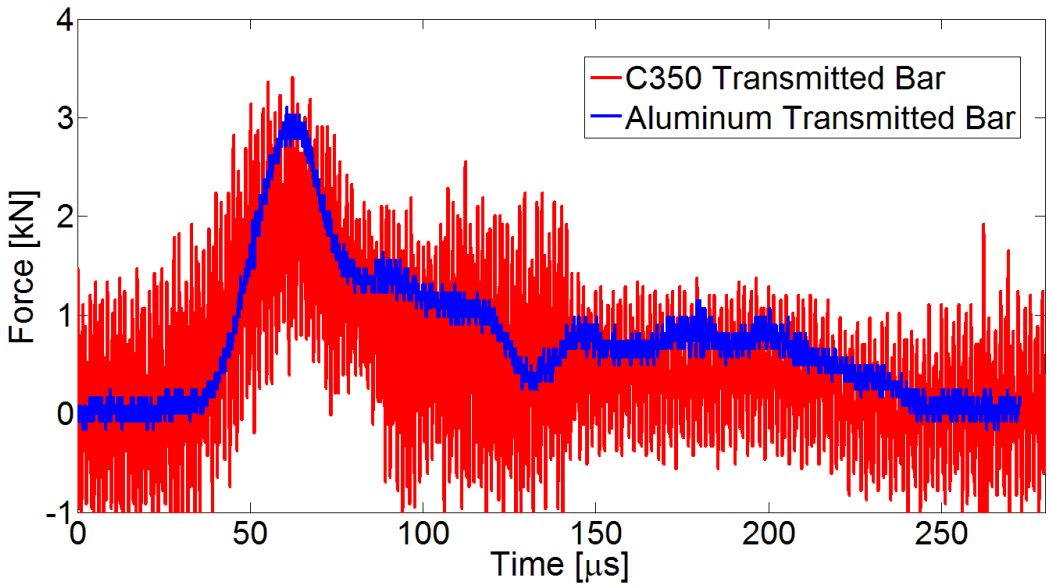

Figure 2.7. Transmitted signal for 10 bead tests with different transmission bar material.

Since the contact area between the bar and bead is small, the high stress concentration there can eventually indent the bar's flat surface. In this case, a pair of platens should be used to protect the bar. The main criterion in selecting the platen material is to ensure acoustic impedance matching between the bar and platens in order to minimize wave disturbances caused by introducing the platens. Tungsten carbide is a material commonly used for platens because of its easy impedance matching with C350 maraging steel. For experiments involving brass and

aluminum spheres, an anvil is not needed because the lower yield strength of the materials does not cause bar indentation. However, anvils are needed when performing tests with stainless steel beads to prevent damage and indentation of the incident bar. Tungsten carbide is placed between the C350 maraging steel and stainless steel specimen, and an aluminum anvil of same bar diameter is used for the transmitted bar to effective act as a replaceable part of the bar. A configuration with both a tungsten carbide and aluminum anvil is shown in Figure 2.8.

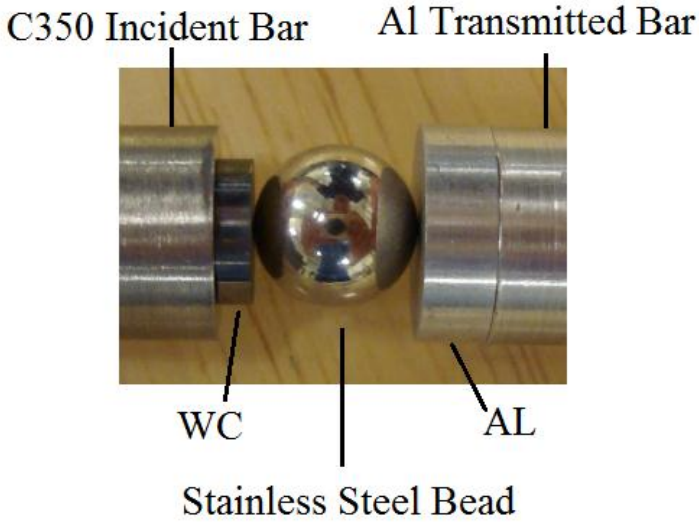

Figure 2.8. Specimen configuration with tungsten carbide and aluminum anvils.

Performing tests on one-dimensional chains of beads requires a support system to maintain one-dimensionality during the test. This requirement is fulfilled by creating a holder, adapted from Spadoni and Daraio (2011), which consists of a hollow metal tube with threaded end caps which can be placed onto the bar. The holders are sized such that at each end a hemisphere extends from the tube and comes into contact with the bar, allowing a point contact between the flat bar surface and the adjacent bead. The edges of the tube are threaded by an end cap of larger inner diameter to ensure the caps will not interfere with the sphere specimens. A schematic of the holder setup is shown in Figure 2.9, and a picture of the holder with one end cap

mounted and one missing is shown in Figure 2.10. The beads are able to slide through the holder without resistance, and post-test observations from the beads inside the holder showed no plasticity caused by lateral expansion into the holder. Chains of beads ranging from two spheres to fourteen spheres were tested with the holder, with different length holder tubes for each corresponding chain length being made. The maximum length of 14 beads that can be tested with this setup is limited by the length of the transmitted bar. When the transmitted pulse reaches the free end of the transmitted bar and reflects back, the signal will be recorded on the strain gage. If this reflected signal from the free end of the transmitted bar overlaps with the signal of the original pulse, then the data will no longer be valid. The length of the transmitted signal is proportional to the length of the chain, which is described in chapter 4, and the maximum length of beads that can be tested in our SHPB without the signals overlapping is fourteen.

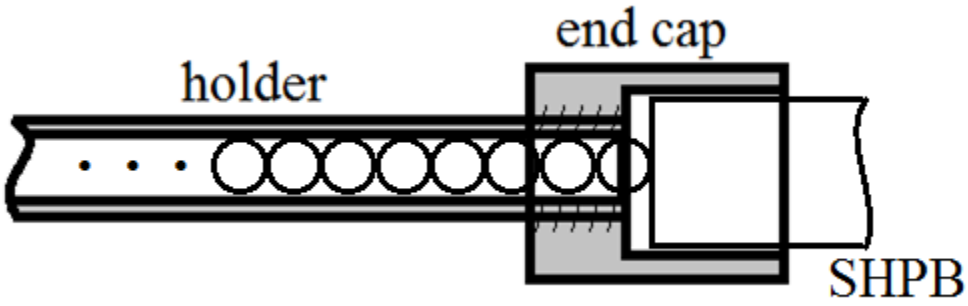

Figure 2.9. Schematic of holder for granular chains.

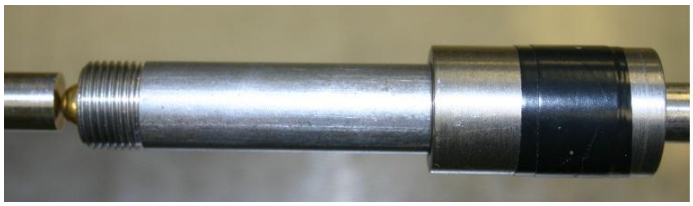

Figure 2.10. Image of the one dimensional sphere holder with one end cap in place.

A typical incident, reflected, and transmitted signal from a 13-bead stainless steel experiment using both a momentum trap and an aluminum transmission bar is shown in Figure 2.11.

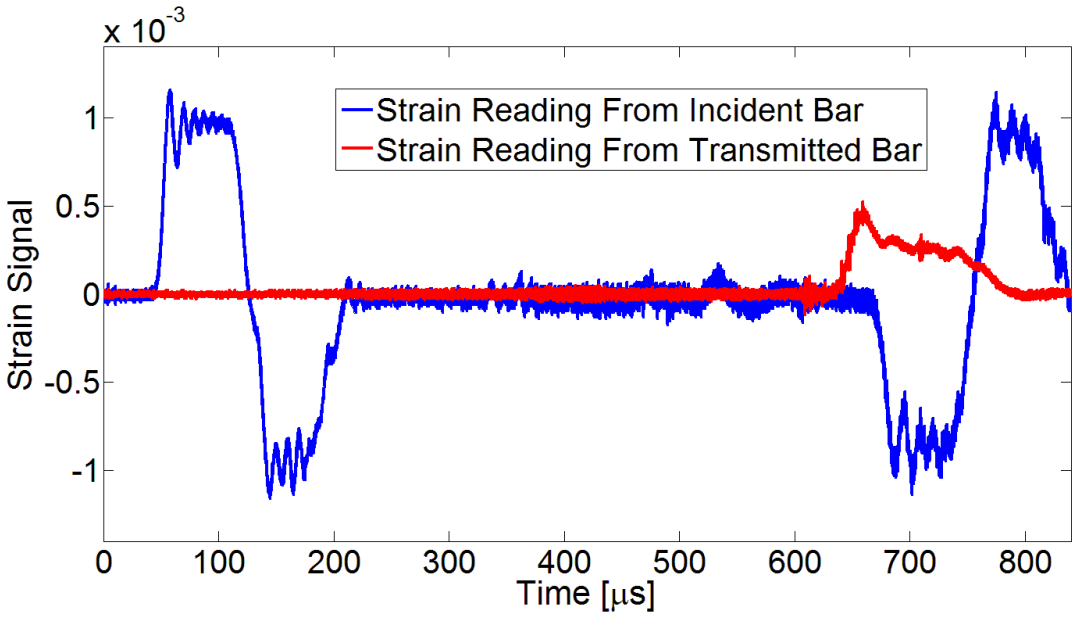

Figure 2.11. Raw incident and transmitted signals acquired from a 13 bead experiment for stainless steel.

Using such data from an array of beads, calculation of the input and output force on the chains can be made through equations (2.1) and (2.2). The engineering stresses and strains are not calculated in the bead experiments because they have no physical relevance. An example of force-in and force-out for a single brass bead is shown in Figure 2.12. The oscillations in the force-in are caused by the oscillations on both the incident and reflected signals. In addition the displacement calculations derived from equation (2.6), can also be made. Figure 2.13 shows the measured front and back displacements from experiments on chain lengths of 1, 5, and 10 beads of brass. The difference between these curves is the net chain compression, δ, illustrated in Figure 1.1b, and is shown in Figure 2.14. Discussion on how to calculate the wave speed, finding

correlations from chain length, and analyzing the evolution of the transmitted signal for the granular chains are analyzed further in chapter 4.

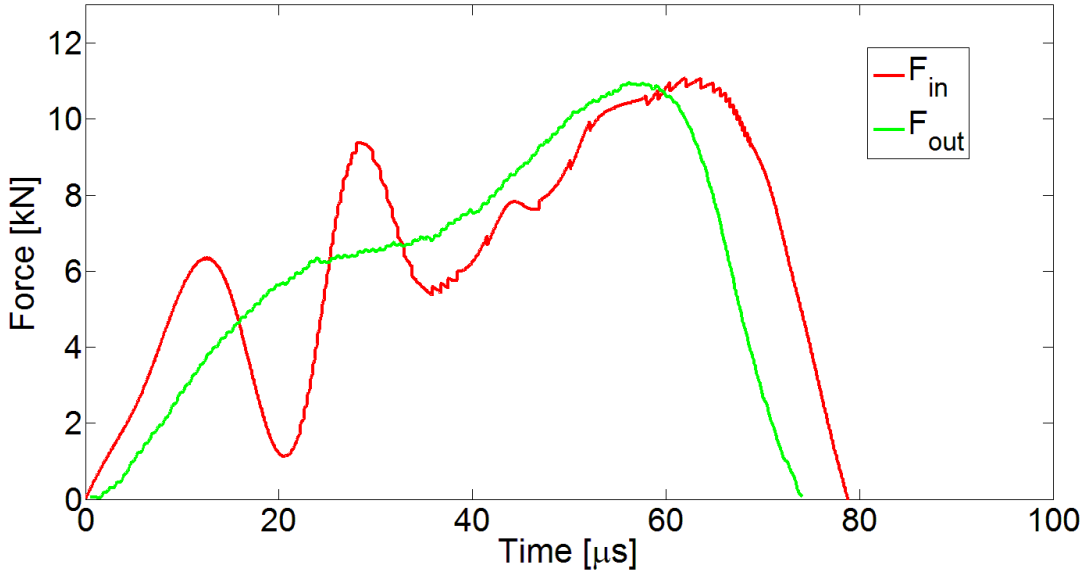

Figure 2.12. Force-in and force-out for a single brass bead.

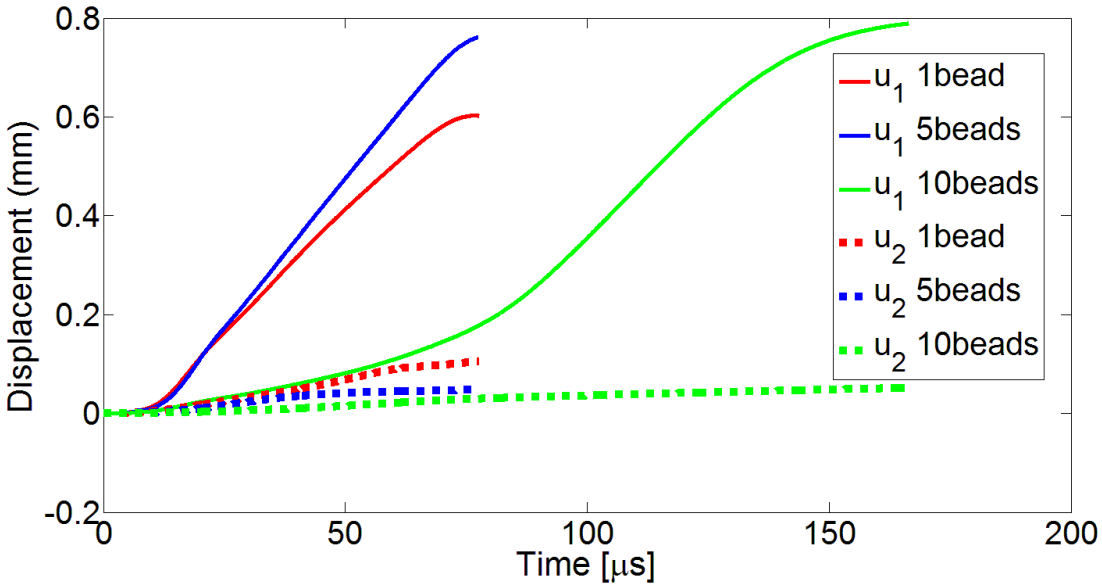

Figure 2.13. Displacement of a brass bead(s) on incident and transmitted interfaces.

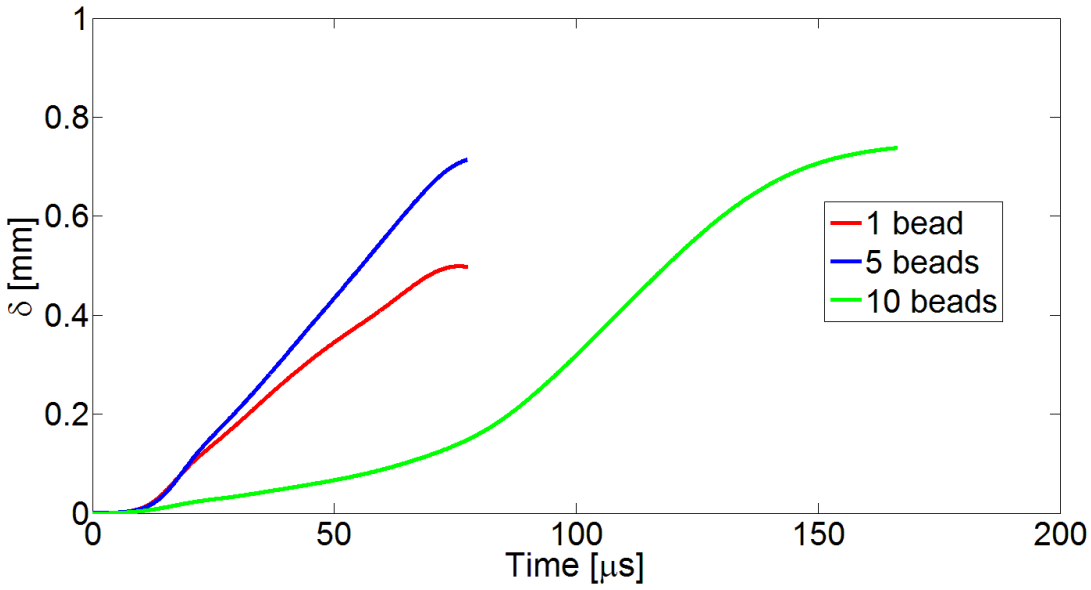

Figure 2.14. Net chain compression of a brass bead(s) experiment.

Chapter 3

Material Characterization

Before evaluating the dynamic response of the granular chains, a process which is meant to probe the details of dynamic load transfer through plastically deforming contact points, it is of interest to know the elasto-plastic constitutive response of the materials themselves that constitute the spheres. Such information will allow us to separate the inherent plasticity nonlinearities from the contact nonlinearities which are also present in the granular system. In addition, precise knowledge of the, possibly rate-dependent, material response would be significant in any future numerical simulations that will be performed. Therefore, it is of interest to perform an initial set of experiments using the SHPB in its traditional role to determine the stress-strain response of the metallic materials used here over a range of loading rates.

3.1 Specimen Preparation

For the granular chains spheres made of brass alloy 260, aluminum alloy 2017, and stainless steel alloy 302 were obtained from McMaster-Carr (www.mcmaster.com). The diameters for all beads are 9.5 mm and the material composition, as supplied by the manufacturer, is given in Table 3.1. Figure 3.1 shows a photograph of one bead from each type of material. Since plastic material response strongly depends on processing conditions which affect microstructural features such as grain size, texture, *etc*., it is important to test the exact material of the beads themselves. Therefore the 9.5 mm diameter beads were machined into cylindrical specimens suitable for traditional SHPB testing. The cylinders were cut via electrical discharged machining from the spheres, with each sphere producing one cylinder of dimensions

6.6 x 3.3 mm (diameter x length). This diameter-length ratio best reduces radial inertia effects in the SHPB (Davis and Hunter, 1963). This size also allows the samples to be tested in both the SHPB and in a traditional servo-hydraulic machine (for static loading) under compression to obtain material properties under different loading rates.

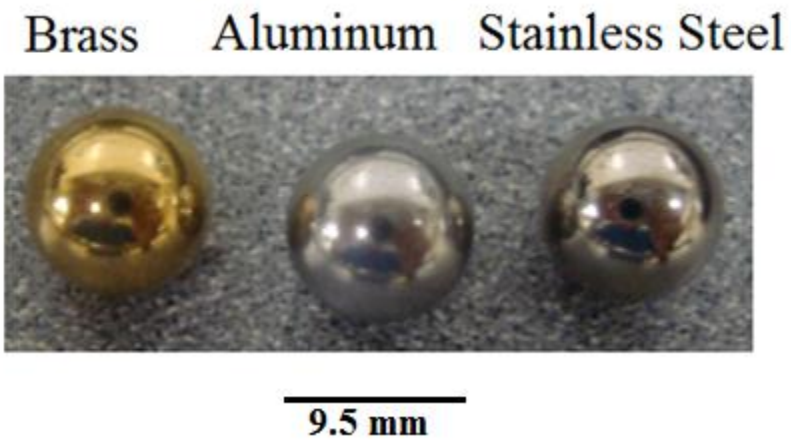

Figure 3.1. Image of 9.5 mm brass, aluminum, and stainless steel bead.

Table 3.1. Manufacturer specification and measured chemical composition in wt %.

	Grade	Cu	Zn	Pb	Fe	Cr	Ni	C	Mn	Si	S	Al
Brass 260	200	70	29.93	0.04	0.03	0	0	0	0	0	0	0
Aluminum 2017	T4	4.1	0	0	0.5	0.1	0	0	0.8	0.6	0	93.9
Stainless Steel 302	100	2	0	0	66.8	18	10	0.06	2.0	1	0.14	0

3.2 Dynamic Homogeneous Material Response

Dynamic testing in the SHPB produced the stress-strain response of the materials subjected to loading rates in the range 1500/s to 3500/s, determined using equation (2.5), and

static tests in the MTS machine loaded the sample at a rate of 0.005/s. Results from a large span of loading rates will show whether the testing materials are rate sensitive or rate insensitive. When loaded in the SHPB, the sample experiences a stress wave on its incident face before the transmitted face, but the cylindrical sample is able to reach a force homogenization after four to five reflections of the stress wave in the specimen. Stress-strain results using equations (2.4) and (2.5) for SHPB tested samples are compared with data from statically tested samples to determine rate sensitivity. Additional force and strain results can be acquired with equations (2.1) and (2.2), which can lead to the variety of results shown in Figure 3.2 and 3.3.

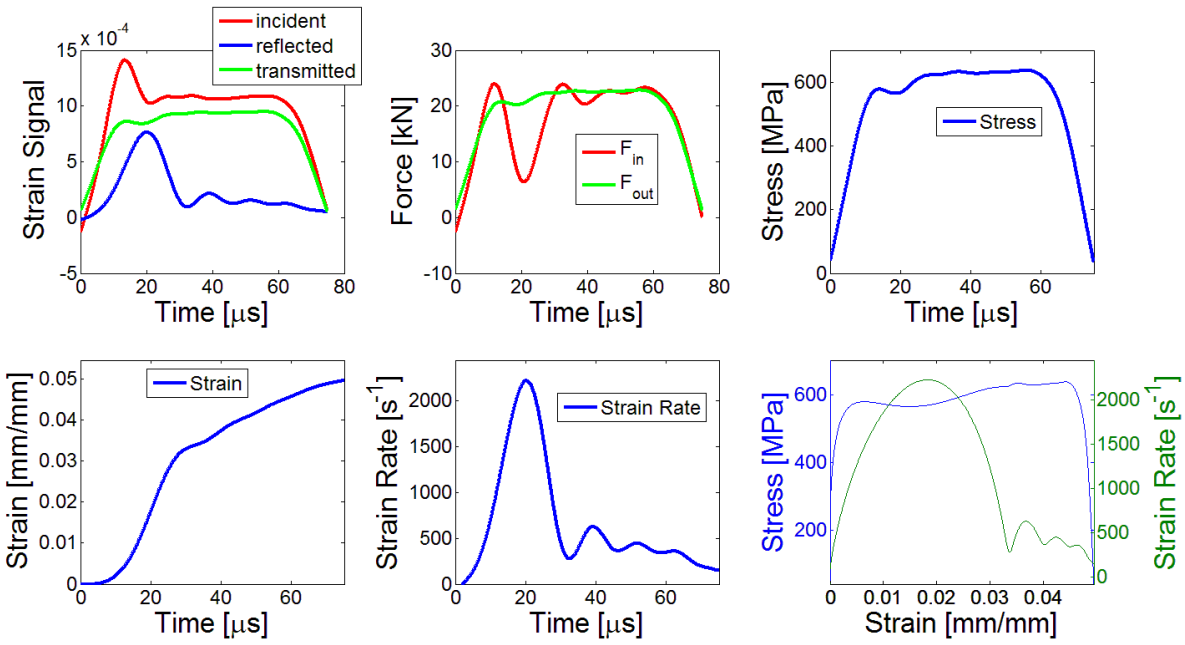

Figure 3.2. Six plot analysis on a brass cylinder.

These figures show six different plots for a brass (Figure 3.2) and aluminum (Figure 3.3) test. The first figure, starting from the leftmost figure on the top row, shows the strain measurements recorded by the strain gages for the incident, reflected, and transmitted pulses for an experiment. Each portion of the signal has been plotted with the same starting time,

corresponding to the time of arrival of the incident wave at the specimen. The middle figure of the top row shows the results of using equations (2.1) and (2.2) to calculate the force input and output of the specimen. The fact that the two forces agree after a certain time confirms that force homogenization indeed occurs during the experiment. The third figure of the top row shows the result of using equation (2.4) to obtain the specimen stress history from the transmitted signal. The middle figure in the bottom row shows the calculation of strain rate during the experiment using equation (2.5). Note that often, depending on the details of pulse shaping, this is not necessarily constant. Integrating the strain rate according to equation (2.5) produces the strain history of the sample, as shown in the left figure in the bottom row. By eliminating time from the stress and strain histories we can construct the material stress-strain curve, as seen in the right figure of the bottom row. Here, the strain rate is also plotted again.

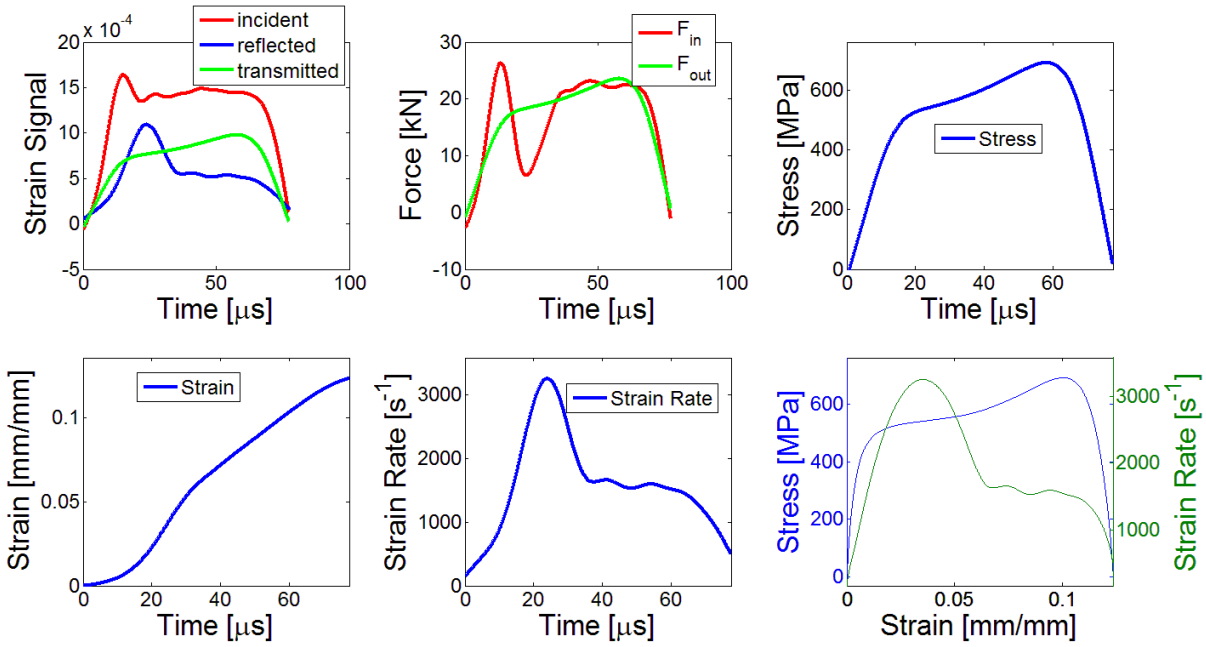

Figure 3.3. Six plot analysis on an aluminum cylinder.

The stress-strain data for aluminum and brass over a range of loading rates are shown in Figures 3.4 and 3.5 respectively. The static and dynamic results for stainless steel were inadequate because the load limit of our instruments was not able to yield the steel samples. For the chosen alloys, both aluminum and brass response appears to be rate insensitive. Furthermore, a power law relation was calculated from the measured stress-strain data as described below.

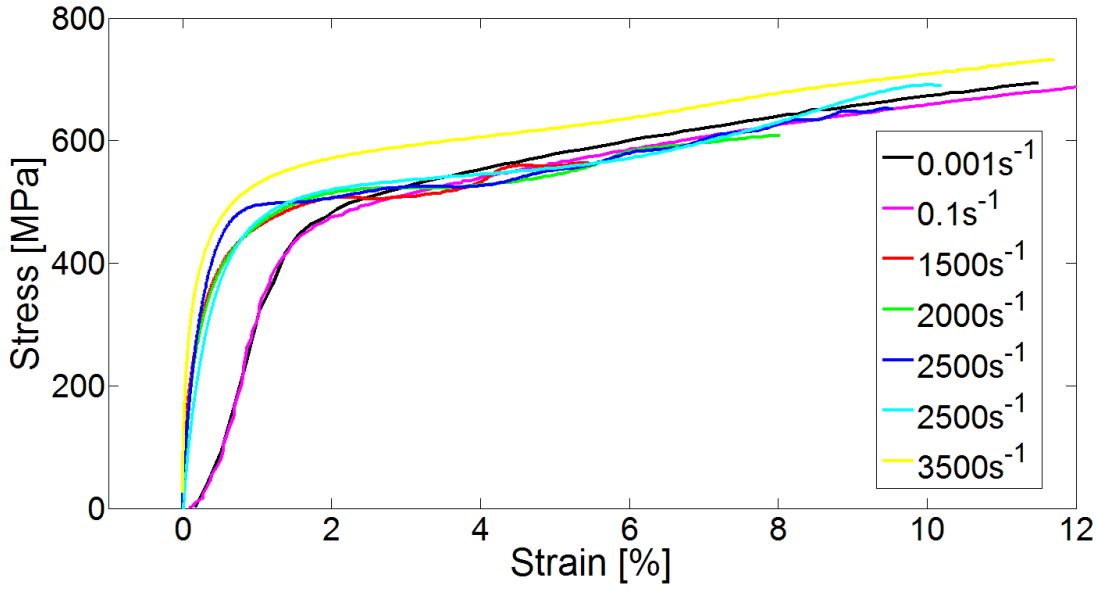

Figure 3.4. Engineering stress-strain curves for aluminum 2017 various loading rates.

(Static result contributed by Erheng Wang)

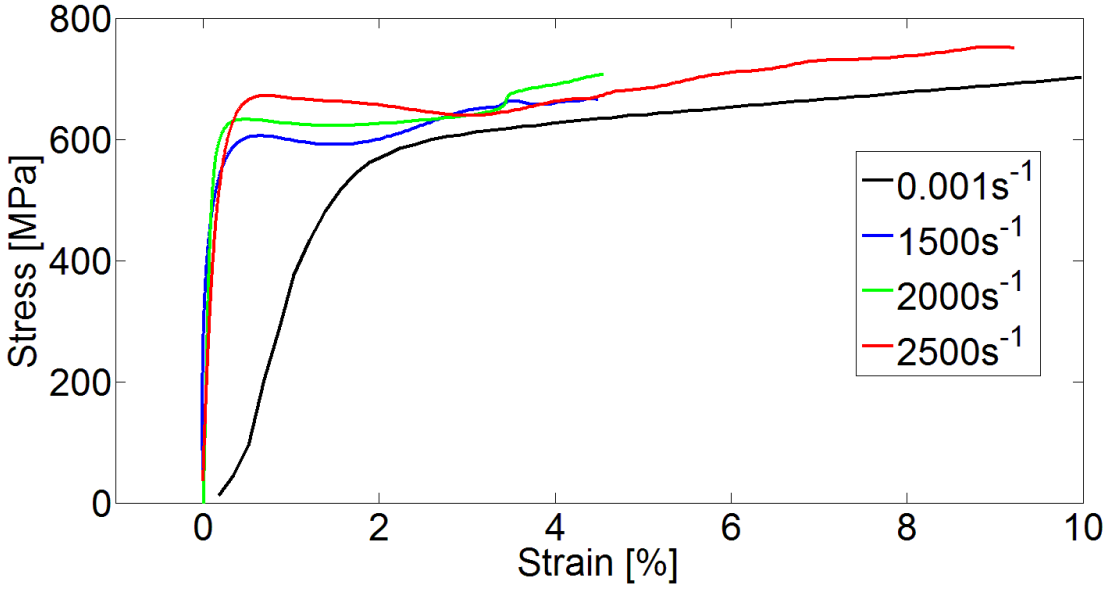

Figure 3.5. Engineering stress-strain curve for brass 260 with various loading rates. (Static result contributed by Erheng Wang)

The Hollomon (1945) analysis was used to find the power law relationship for the test materials. This analysis assumes the stress-strain curve is described by the power relationship:

$$\sigma_t = A\varepsilon_t^n \tag{3.6}$$

where σ_t and ε_t are the true stress and true strain of the material and n is the strain hardening exponent. Ductile metals at room temperature usually exhibit values of n from 0.02 to 0.5. This fit was applied to both the aluminum and brass samples and resulted in the power law relations in Figure 3.6 and 3.7, where n = 0.14 and 0.06, respectively. The strain hardening exponent is also correlated with the rate sensitivity of the material, with a larger value corresponding to a more rate sensitive material. Resulting values for both aluminum and brass agrees that both materials are rate insensitive, which is taken into consideration when adapted to testing for granular media.

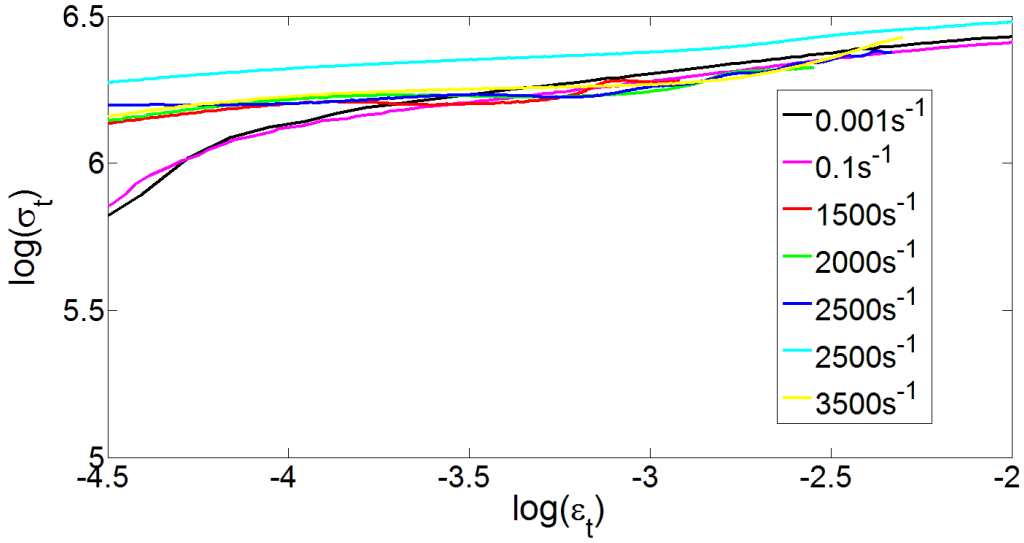

Figure 3.6. Power law representation of the plastic stress-strain relation for aluminum 2017 with an average strain hardening exponent of 0.14.

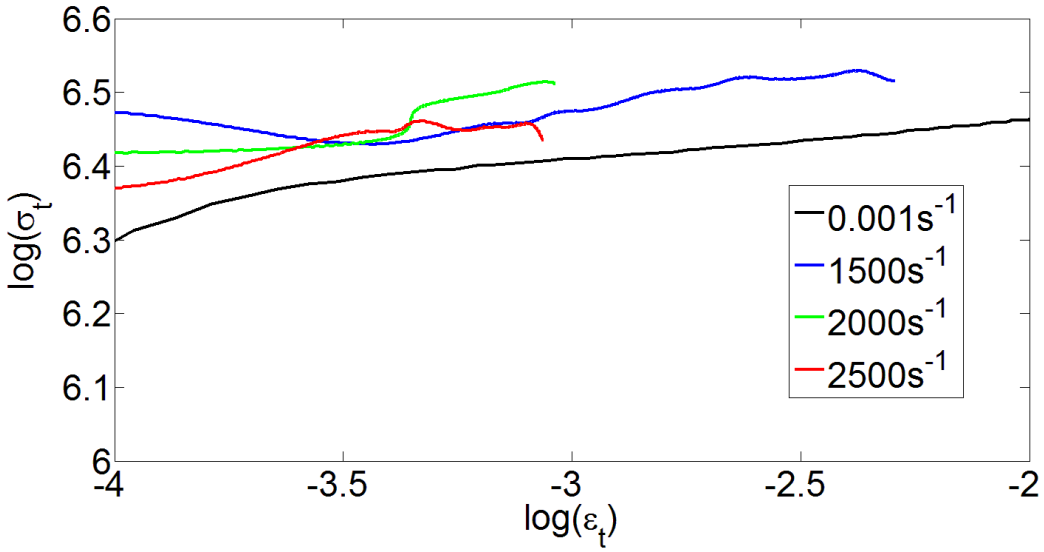

Figure 3.7. Power law representation of the plastic stress-strain relation for brass 260 with an average strain hardening exponent of 0.06.

Chapter 4

Dynamic Loading of Homogeneous Granular Chains

4.1 Formation of Solitary Waves in Brass

In this section we will concentrate first on results from the experiments on arrays of brass beads, as brass is the easiest material to work with. However, similar results were seen for other metals such as aluminum and steel. These are presented in section 4.2.

It has been known that the dynamic response of elastic granular media in the strongly nonlinear regime can support solitary waves. These solitary waves are lumps of energy which Nesterenko (2001) found to be spanning the wavelength of approximately five particles in a spherical particle chain. In this work we are interested in investigating whether such strongly nonlinear solitary waves can exist in granular chains subjected to high loads and loading rate.

4.1.1 *Solitary Wave Development with Increasing Chain Length*

Specimen bead chains comprised of brass were tested at various lengths spanning from a single bead up to twelve beads. The resulting transmitted stress wave propagating through the beads was recorded by the transmitted bar strain gage. Single brass beads were initially tested. These results can be compared, as shown in Figure 4.1, to those from a cylindrical specimen used for obtaining the stress-strain curves, to view how the stress wave differs with the specimen homogenization. This figure compares the transmitted signal of a single bead and a cylindrical sample, both from the same material and loaded at approximately the same rate. Since both tests were loaded with almost identical inputs, as shown in Figure 4.2, their comparison can be a valid

approach to finding major differences between the two signals. The brass cylinder was cut from a brass bead, as stated in chapter 3, limiting the size of the cylinder. The actual volume of the cylinder is 60 percent of the sphere, but the differences in the transmitted stress wave are caused by another factor. The limited contact area between the flat bar surface and the spherical specimen changes the stress wave that propagates through the sphere. Since a cylinder has a large, flat area in contact with the bar, an almost planar stress wave is transmitted into the cylindrical specimen. In contrast, the limited contact area of the sphere with the bar, although increasing throughout the experiment, generates a transfer of load from the linear element (bar) into the nonlinear element (sphere) similar to that corresponding to a point load indentation. This effect has also been seen in cylinders in contact as shown by the photoelastic measurements of Sadd *et al.* (1992).

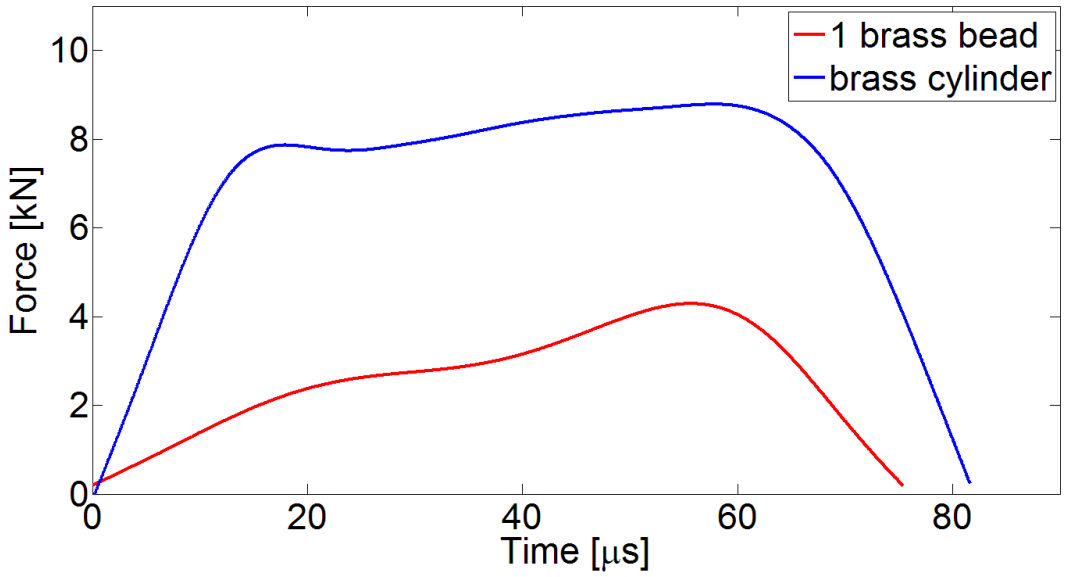

Figure 4.1. Transmitted signal of a brass bead and a brass cylinder.

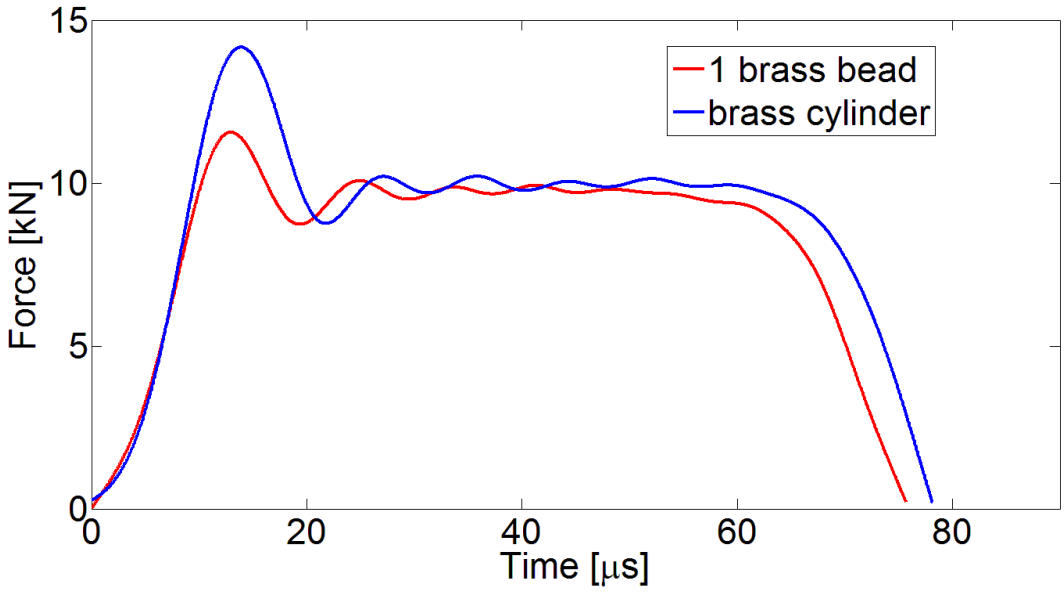

Figure 4.2. Loading pulses from the brass bead and brass cylinder samples from Figure 4.1.

Comparing data from four single bead experiments in Figure 4.3, we see that the shape of the transmitted stress wave is quite repeatable. These four tests, shown by four separate colors, were loaded with an input pulse of similar shape and magnitude. Note that each single bead signal contains two peaks, which occur at a similar time among the four tests. The duration of each signal is also the same. Based on the experiments of two contacting hemispheres that show only one such peak (Wang and Lambros, 2011), it is deduced that the two peaks correspond to successive yielding of the front and back contact points on the single sphere. The unloading occurs because the limited loading pulse duration.

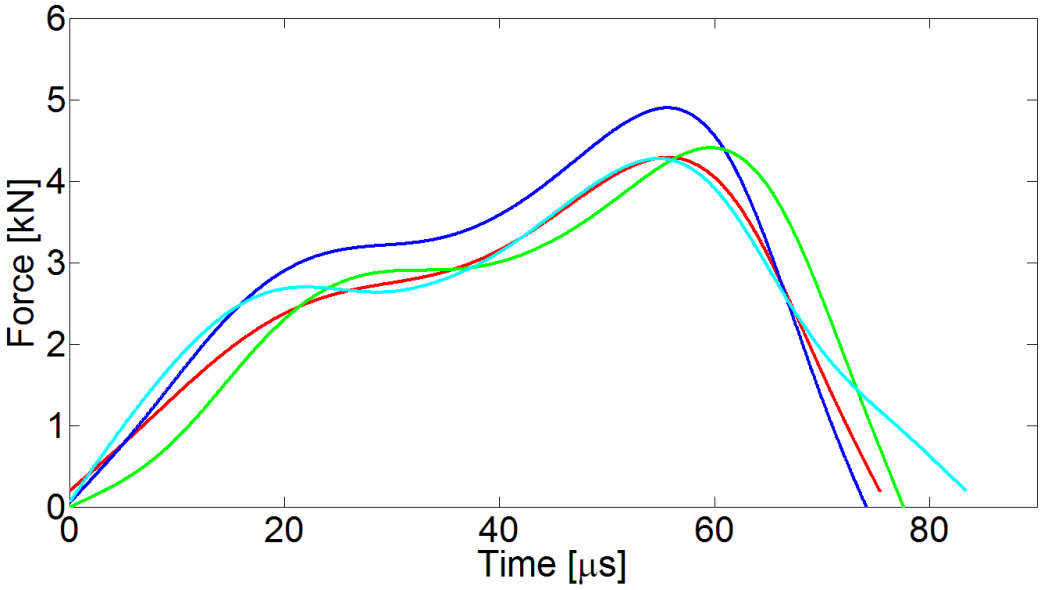

Figure 4.3. Four transmitted signals from single beads with similar loading pulses.

As the number of beads in the chain increases, the stress wave which propagates through it begins to evolve beyond the two-yield form shown in Figure 4.3. The duration of the transmitted pulse increases as the chain length increases, as is seen in Figure 4.5 which shows the transmitted signal for bead chain lengths of one to five beads – five beads being the necessary number for the formation of a solitary wave in the elastic case. Even though the input load (Figure 4.4) is of the same 80 μs duration in all cases, although not necessarily the same amplitude, the resulting transmitted pulse (Figure 4.5) is variable, partially attributable to the limited contact area between spheres. Note that the transmitted pulse duration for chains with two or three beads, is shorter than that of a single bead, and of the loading pulse duration. This result was seen consistently for repeated tests of two and three beads, and the reason for it is not clear. However, this "transition" occurs at the same time as the amplitude of the first and second peaks reversing in magnitude, as seen in Figure 4.5. The two peaks, which are thought to correspond to the yielding of individual contact points, also begin to converge into a single peak.

This becomes apparent in the four, and especially the five, bead case. As the number of beads increases, the transmitted pulse also begins to attain a trailing pulse of lower amplitude.

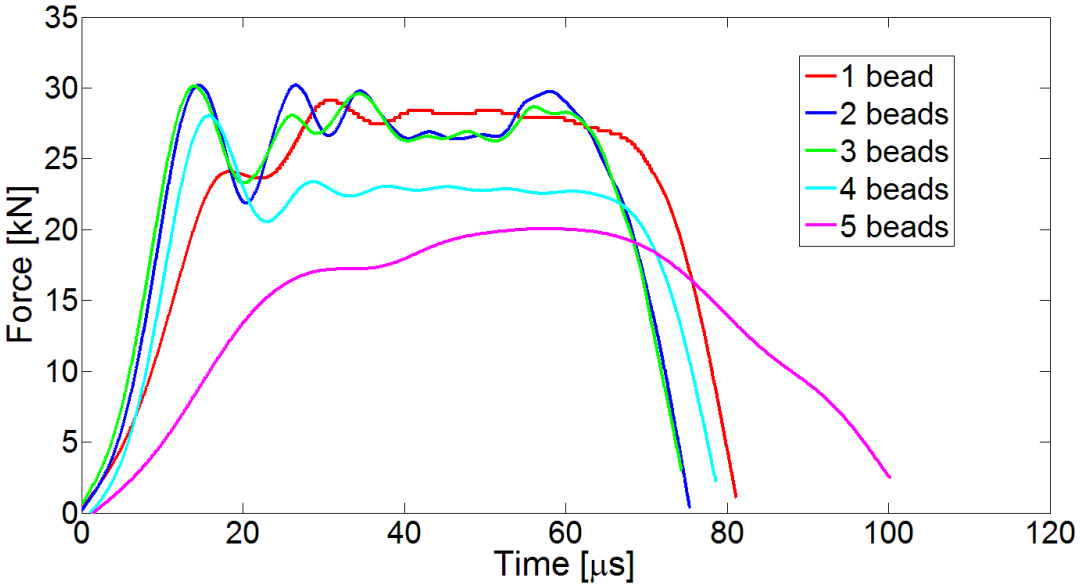

Figure 4.4. Incident signals for brass bead chains of length one through five.

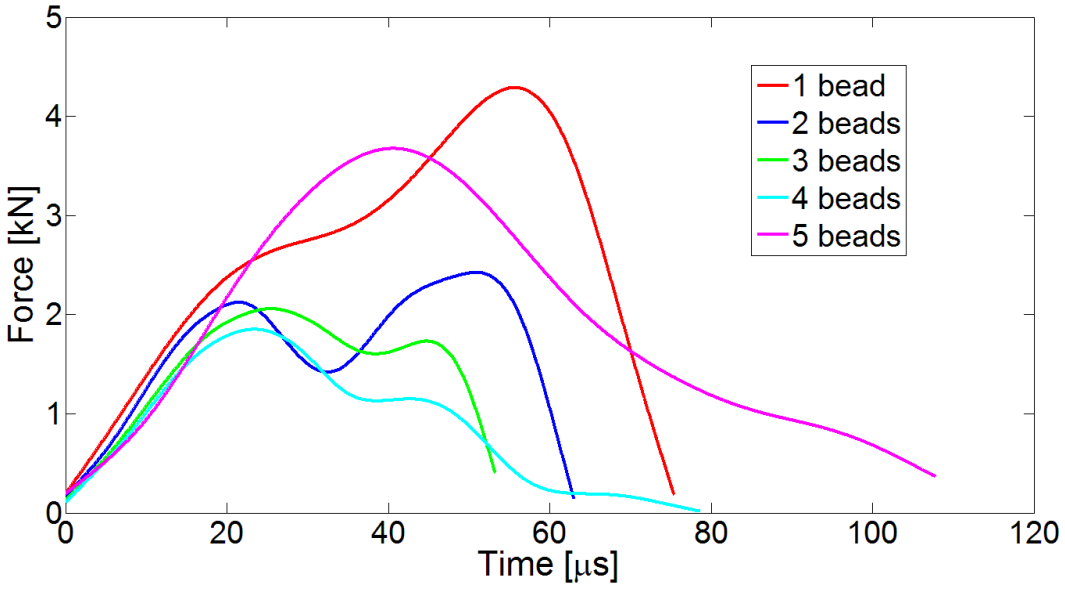

Figure 4.5. Transmitted signals for brass bead chains of length one through five.

This trailing wave is more apparent in Figure 4.7, which shows the transmitted pulse for longer chains of beads, from five (same curve as that in Figure 4.5) to twelve brass beads in length. The duration of the transmitted stress wave increases as the granular chain length increases. This phenomenon does not appear for a cylinder of increasing length where the duration of the transmitted signal is not affected by the length of the specimen, but rather is controlled only by the incident loading duration. The increasing duration of the transmitted signal in the granular case is produced by a combination of the nonlinear contact between beads and the effect of plasticity, and may be useful in stress wave management and mitigation applications. Figure 4.6 shows the corresponding input for these transmitted signals. By comparing the amplitude of these incident pulses, it can be seen that the magnitude of the transmitted force decays with chain length. This can be attributed to the additional plasticity involved with the additional beads, which will lower the signal that reaches the transmitted bar.

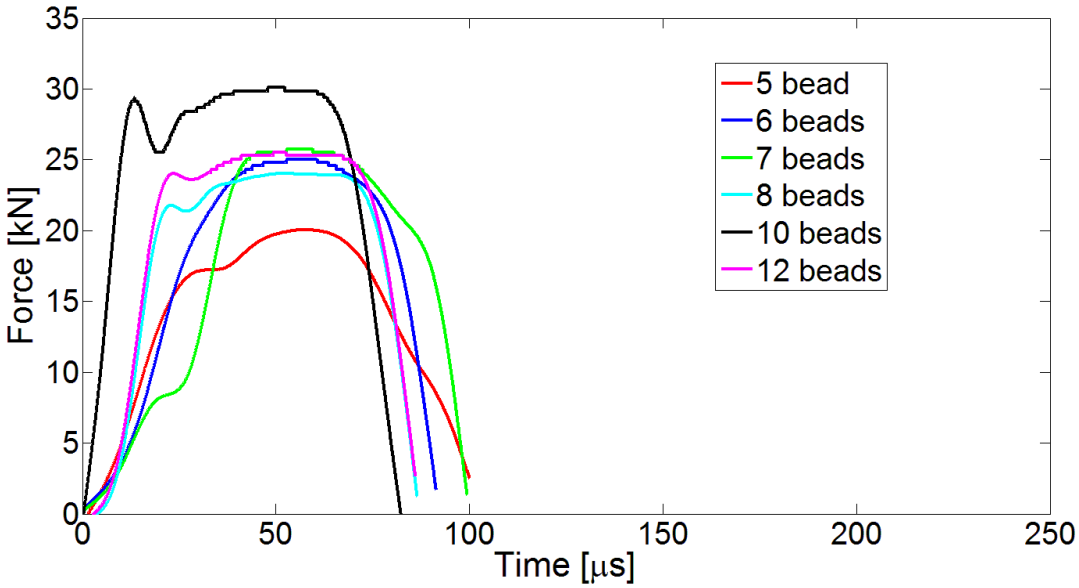

Figure 4.6. Incident signals for brass bead chains of length five through twelve.

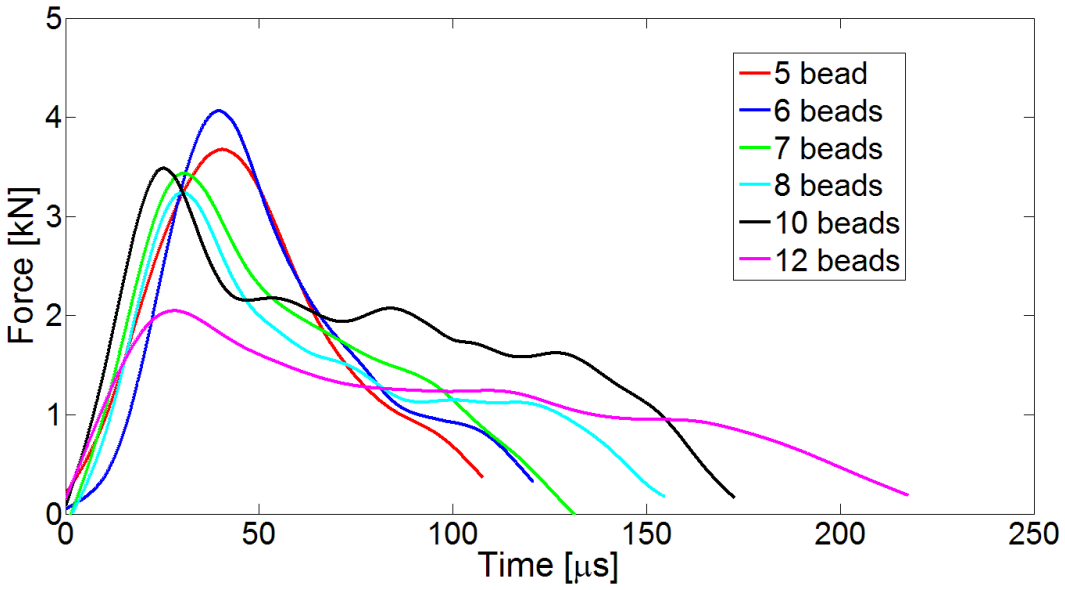

Figure 4.7. Transmitted signals for brass bead chains of length five through twelve.

The time when the transmitted signal first appears is not the same for different chain lengths; the previous two figures placed an offset to the initial point to better view the evolution of the stress wave with length. The actual transmitted signals shown in Figure 4.8 have different starting points for different lengths. Clearly, a longer chain will result in a longer time delay, corresponding to an increased travel distance of the transmitted wave. However, for the linear elastic case it is known that another property of solitary waves is that they travel at an amplitude-dependent speed rather than a fixed wave speed. Specifically, as was mentioned in the introduction, in the elastic case the solitary waves travel at speeds according to equation (1.2), *i.e.*, the wave speed is proportional to the 1/6 power of the maximum force. To investigate the possible force dependence of the wave speed, the results shown in Figure 4.8 are for experiments with similar impact forces, within the range of controllability of the SHPB device. Specifically, the test results shown in this figure were subjected to an incident loading pulse between 18 kN

and 25 kN. The clear time delay, which increases with bead length, is examined further when calculating the wave speed propagating through the chain as discussed in the next section.

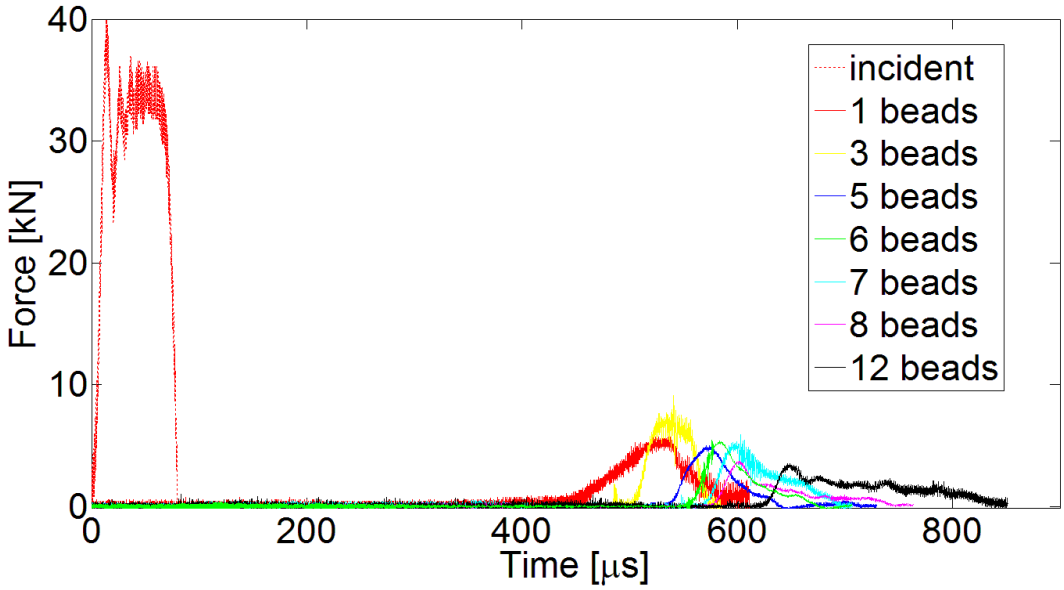

Figure 4.8. Unaltered signal for brass beads of various chain lengths.

4.1.2 *Wave Speed Calculations*

In traditional one-dimensional dynamic plasticity theory (*e.g.*, Lubliner, 1990), a propagating elasto-plastic wave has an elastic precursor and a plastic wave component travelling at a slower speed than the elastic precursor. The elastic precursor travels at $c_o=\sqrt{E/\rho}$ while the plastic wave travels at speeds $c_p=\sqrt{E_t/\rho}$ where E_t is the tangent modulus schematically shown in Figure 4.9, which varies depending on the current yield stress. In the case of the granular medium of interest here the force displacement relation is schematically illustrated by the (elastic) Hertzian contact law in Figure 1.1. In this figure it is clear that since the initial slope is zero, there should be no elastic precursor analogous to c_o. This is referred to as a sonic vacuum.

Note that this contact law, or in our case its plastic equivalent, is valid only if inertial effects in the beads are neglected, *i.e.*, the beads are under homogenous conditions. Therefore, generally no elastic precursor is expected here, at least if a solitary wave is to form. Even in the event that the dynamic homogenization conditions do not hold, it is likely that the elastic precursor, travelling at speed c_d of the material, will be very small.

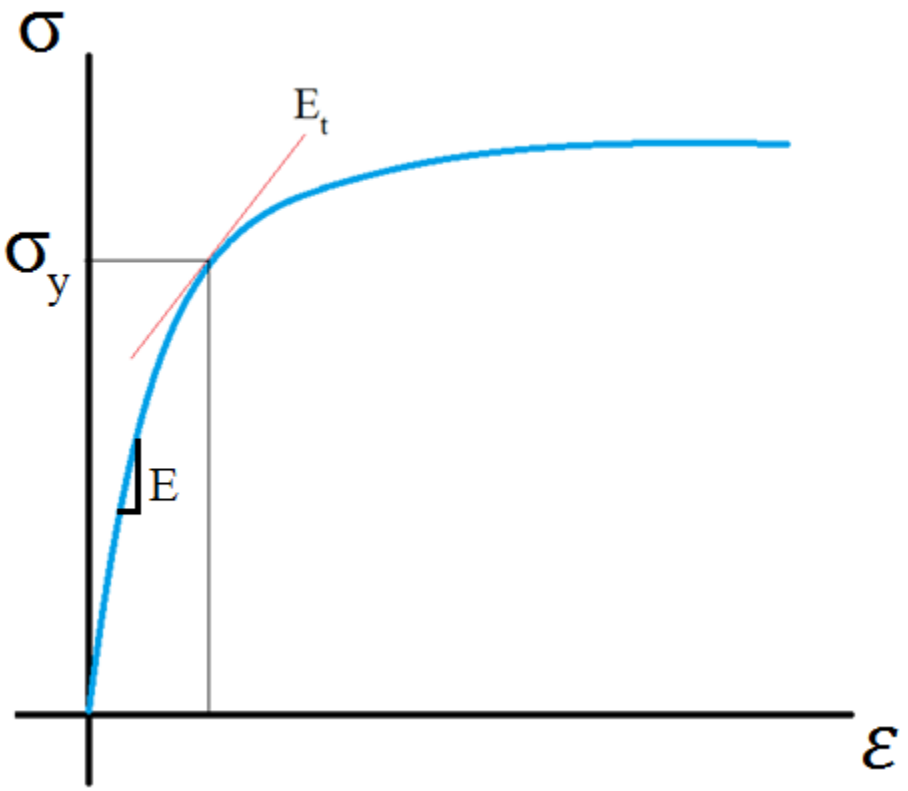

Figure 4.9. Stress-strain curve displaying the tangent modulus at yield.

Using the strain data in the SHBP, the plastic wave speed can be calculated using the equation

$$V = \frac{2N*a}{t_{total} - t_{inc} - t_{trans}}. \tag{4.1}$$

This simplified velocity V is the shortest linear distance along the entire chain of beads divided by the elapsed time of the propagating stress wave in the chain. N denotes the number of beads in the chain, a is the diameter of the bead, and t_{total} is the time duration starting when the incident strain gage receives a signal and ending when the transmitted strain gage receives a signal. The travel time of the stress wave within the chain can be calculated by knowing the positions of the strain gages and the elastic wave transit time from between these locations and the incident and transmitted bar ends in contact with the chain. Since the material of the bar and the gage positions are known, both the wave velocity of the bar and the distance from the strain gage to the specimen can be calculated. This results in the travelling time of the wave within the incident bar and transmitted bar, which are denoted as t_{inc} and t_{trans}, respectively. Thus, the denominator in equation (4.1) represents the travelling time of the stress wave that propagated through the chain. This wave speed is plotted against the chain length in Figure 4.10. Another attempt to find the travelling time of the wave was to measure the time between the peak of the loading pulse and the peak of the transmitted pulse. The purpose for using the peaks is to gauge the time of travel for the maximum amplitude of the wave. However, signals with multiple peaks, as shown in Figures 4.3 and 4.5 caused problems on the selection of the correct peak; therefore, the time of arrival of the wave is used instead.

The plastic wave speed calculated in a single bead has significant variation compared to longer chains, which might be caused by the unrepeatability in the yielding time. Also a measurement error of just one microsecond would cause a total speed error of 50 m/s in a single bead. This error is not enough to compensate for the large differences in the wave speed for a single bead. However, the same one microsecond measurement error would equate to a total speed error of only 4 m/s for a chain of ten beads. For a certain load range, it can be seen in

Figure 4.10 that the wave velocity begins to level off, which might be caused by the formation of the solitary wave. This leveling zone appears to start around five beads in length, similar to the length of the elastic solitary wave.

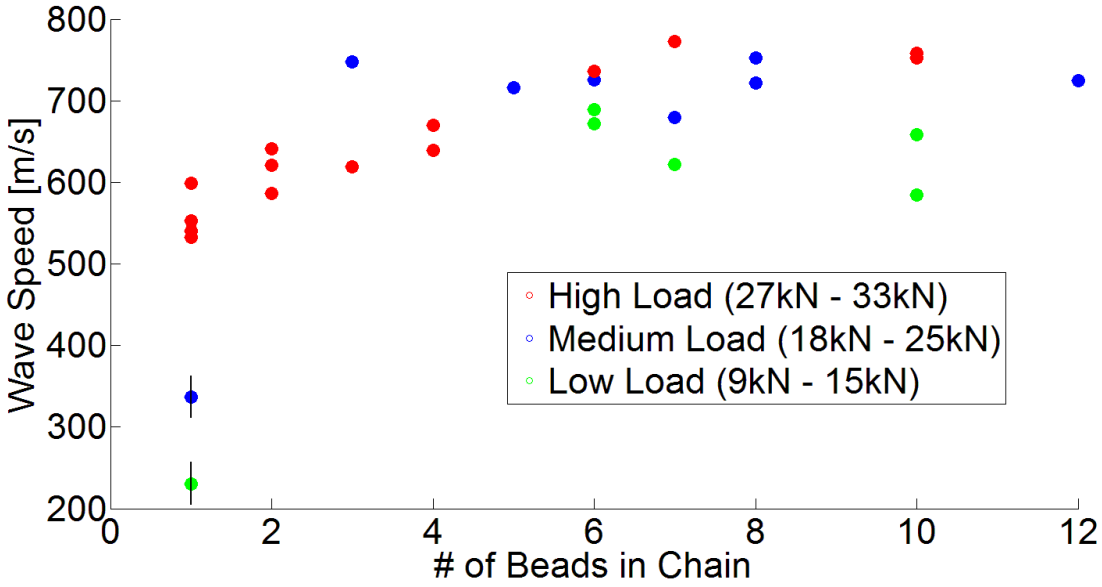

Figure 4.10. Plastic wave speed through one-dimensional brass beads of various chain lengths.

However, the solitary wave speed also depends on loading amplitude. It is expected that a larger force will result in a faster wave, as is the case for the elastic solitary waves. To better isolate the effects of loading magnitude, different loading inputs for a set chain length are displayed in Figure 4.11 and Figure 4.12 for six and ten bead chains respectively. Aside from the magnitude of the incident pulse causing a direct correlation with the magnitude of the transmitted pulse, the rise time for the transmitted pulse is faster for a larger input load than its lesser counterpart. Comparing the 21 kN and 13 kN signals in the chain of six beads, both display similar incident loading rates, but the transmitted loading rate differs: a higher load magnitude causes a higher loading rate. The onset for the maximum signal in the transmitted

pulse is also affected by the loading signal. The stronger input caused the peak of the transmitted signal to occur earlier, which correlates with the faster wave speed.

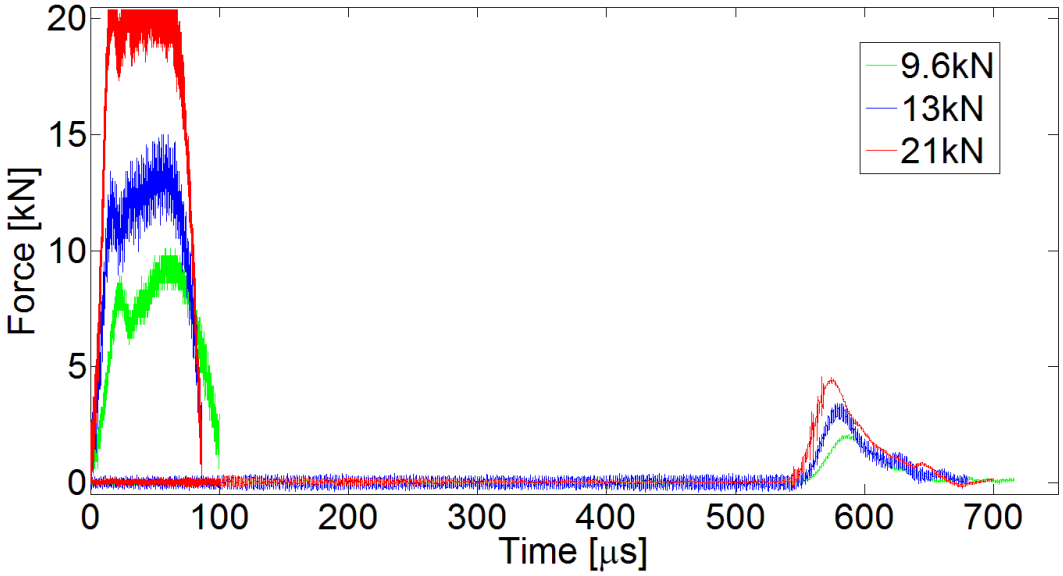

Figure 4.11. Loading and transmitted data for brass chains of six beads.

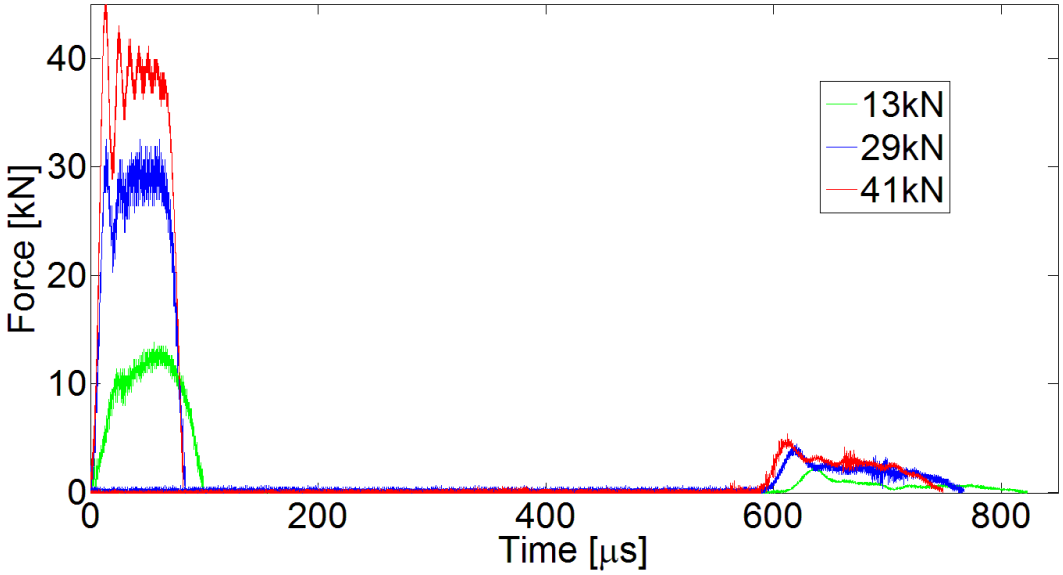

Figure 4.12. Loading and transmitted data for brass chains of ten beads.

Nesterenko (1984) described solitary waves forming under a chain of identical elastic beads with the velocity also scaling with $F_{max}^{1/6}$ when no initial precompression occurs. This relation is compared to the experimental brass chains, which consists of identical beads that

deform plastically under zero precompression. The measured wave speed for chains of more than five beads only are plotted against both the maximum incident force and the maximum transmitted force in Figure 4.13 and Figure 4.14, respectively. A power law fitted to the experimental data is compared to that of 1/6 power which is calculated by equation (1.2). In both comparisons, with the incident and transmitted forces, the experimental velocity scales less than $F_{max}^{1/6}$, approaching $F_{max}^{1/9}$ instead. This is likely an effect of plasticity which can have additional damping effects on the solitary wave generation. However, it is clear that the speed does depend on either input or output force, denoting that a nonlinear solitary wave is propagating after chain lengths of five beads.

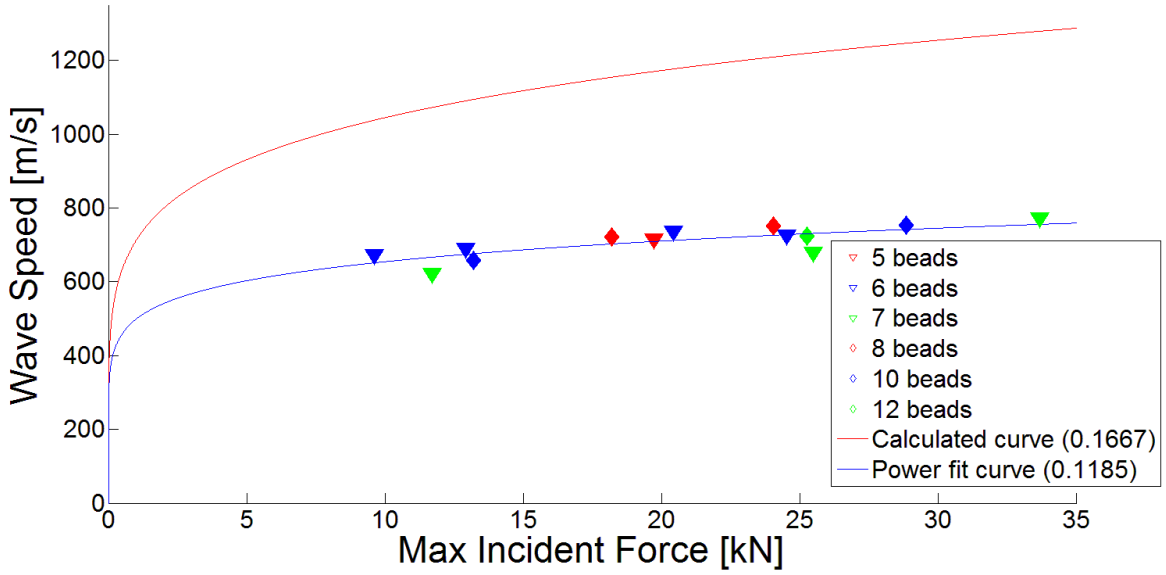

Figure 4.13. Wave speed vs. maximum incident force for various brass bead chains.

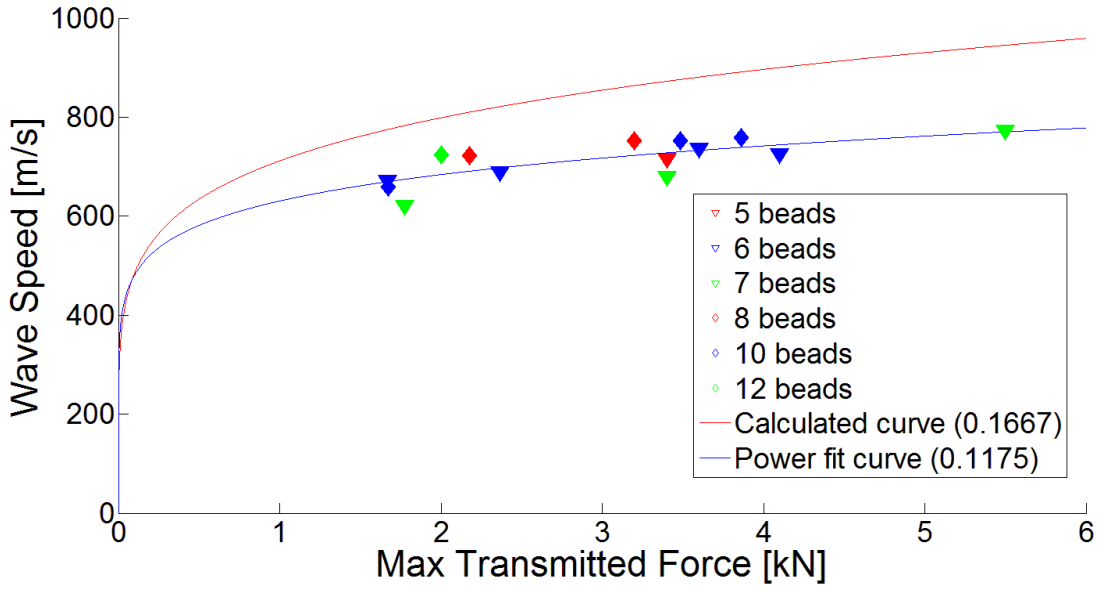

Figure 4.14. Wave speed vs. maximum transmitted force for various brass bead chains.

4.1.3 *Plastic Dissipation Along the Chain*

Since these granular chains are impacted under high loads, the brass beads undergo permanent plastic deformation. This deformation can be measured and studied to determine additional characteristics of energy dissipation along the granular chain, as opposed to only the global measures of transmitted force and wave speed discussed in the previous sections. The amount of plasticity a bead undergoes can be quantified by the area of the circularly deformed face on each side of the bead resulting from the plastic contact with its neighbors. Since this measurement is a postmortem examination, precautions are needed to ensure the measured deformation corresponds with the experiment. One possible error of such plasticity measurements is multiple impacts from reflections in the incident bar, which will cause successive reflections to compress the bead chain more than once. To eliminate such reflections, the momentum trap is used in every test, which ensures single pulse loading every time.

However, even with the presence of a momentum trap, multiple hits can be seen on a face of a bead, as exemplified by Figure 4.15 which shows a microscope image of multiple yield indents. The ring pattern is caused by the machining surface of the bar. The primary impact caused the larger of the deformations, while residual waves within the chain caused the smaller dent. These multiple impact zones are only present on the boundary beads which are in contact with either the incident or transmission bar, and are likely results of rebounds of the end beads onto the SHPB bars. Beads within the chain do not show noticeable signs of multiple impacts. This shows the energy of the reflections within the chain is able to compress a bead into a bar with which it was no longer in contact.

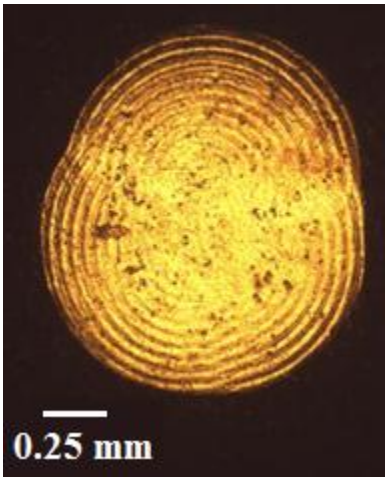

Figure 4.15. Microscope image of a brass bead with multiple impact sites.

To compare the magnitude of plasticity that occurs within a chain of beads, the yielded areas are measured. This measurement is done by taking images of the deformed bead under a microscope, and measuring the yielded area by comparing the image with a scale. The average measured diameter at several locations is used to determine the area, as shown in Figure 4.16. In cases where multiple impacts are present, the largest deformation is taken as the yield caused by the primary stress wave. These yielded areas for several tests are plotted in Figure 4.17 as a

function of location along the chain. The location along the chain represents the position of the yielded face. The first data point corresponds to the yielded face of bead #1 in contact with the incident bar, while the second data point corresponds to the opposite face on bead #1. The third data point corresponds to the face on bead #2 which contacts bead #1, and so on. In theory the residual contact areas of adjacent beads on their common contact surface should be equal. However, it is difficult to decide which two faces of different beads are adjacent because their yielded area measurements are not necessarily the same. Therefore although each bead was numbered with its location along the chain we cannot definitively identify which side of the bead was facing the loading side of the granular chain. Therefore in the plots of Figure 4.17 the beads have been placed such that adjacent contact areas are as close as possible. Clearly, the plasticity in the middle of the chain is less than the plasticity closer to the edges for short chains, especially noticeable for the four bead tests displayed in red and blue in Figure 4.17. (Recall that the first and last measurement point in each curve corresponds to the beads in contact with the bar and contain evidence of multiple impacts.) Perhaps surprisingly, since a monotonic decrease of force, and therefore plastic dissipation, along the chain may be expected, the plasticity along the chain for short lengths is varying. Thus, the propagating stress wave appears to also vary as the solitary wave develops. However, for longer chains the early part of the data is monotonically decreasing, denoting a well-established solitary wave of decreasing amplitude.

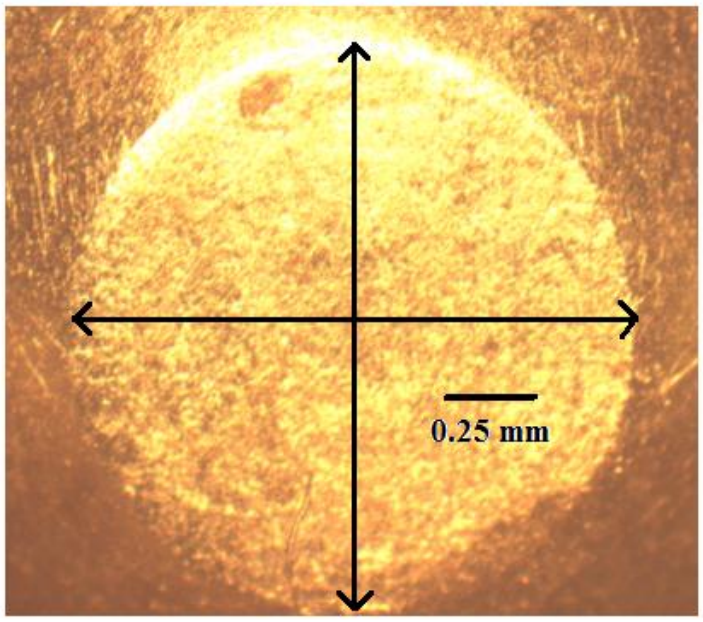

Figure 4.16. Microscope image of deformed area with diameter lines.

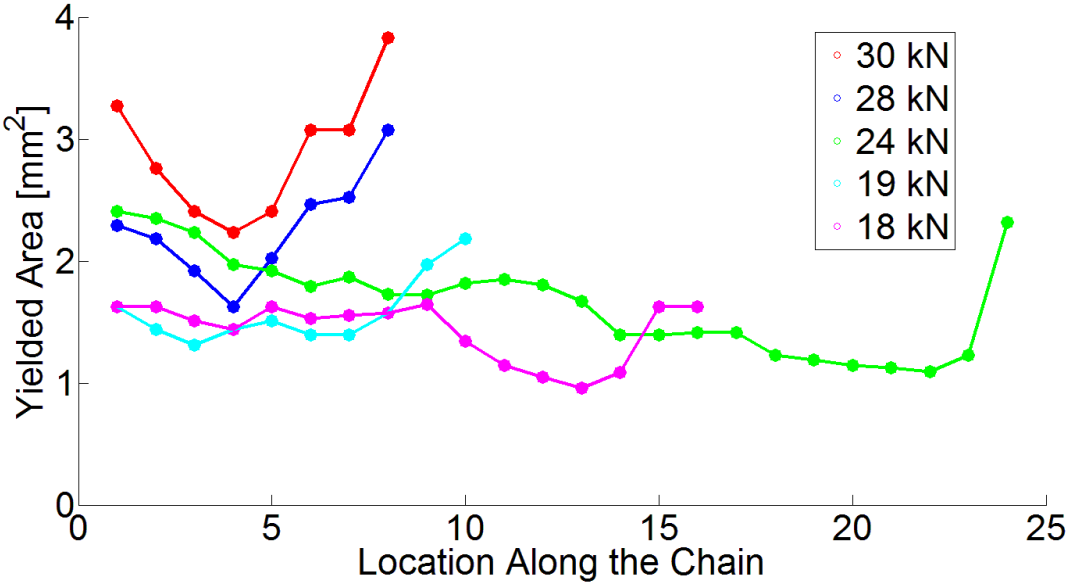

Figure 4.17. Yielded areas of brass bead chains of lengths four through twelve.

4.2 Effects of Material

Aluminum 2017 and stainless steel 302 were also tested in addition to brass 260. The results from testing homogeneous chains of these materials are presented in the following sections. Generally the results follow the same trends as those above. One important difference, however, is that although the brass and aluminum materials are rate insensitive, the steel 302 is rate sensitive (Wang and Lambros, 2011). It is of interest to investigate what effects such material rate sensitivity will have when coupled with the convex nonlinearity of the contact law and the concave nonlinearity of the plasticity response.

4.2.1 *Aluminum (Alloy 2017)*

Although fewer aluminum tests were conducted than brass, trends apparent from the aluminum results can be compared to those from brass. Figure 4.18 shows the transmitted signals for different lengths of one dimensional aluminum granular chains, indicating a similar trend to the brass chains. Of course once again additional beads in the chain length increase the delay of the transmitted signal and the amount of extra transit time required can be linked with the chain wave speed. These transmitted aluminum signals have a force which is present over a longer duration with multiple peaks, whereas the brass transmitted pulse contained a short, single peak, as seen by comparing Figures 4.8 and 4.18. The aluminum data also shows less of a trailing signal after the peak, indicating that in this case the material produces less dissipation.

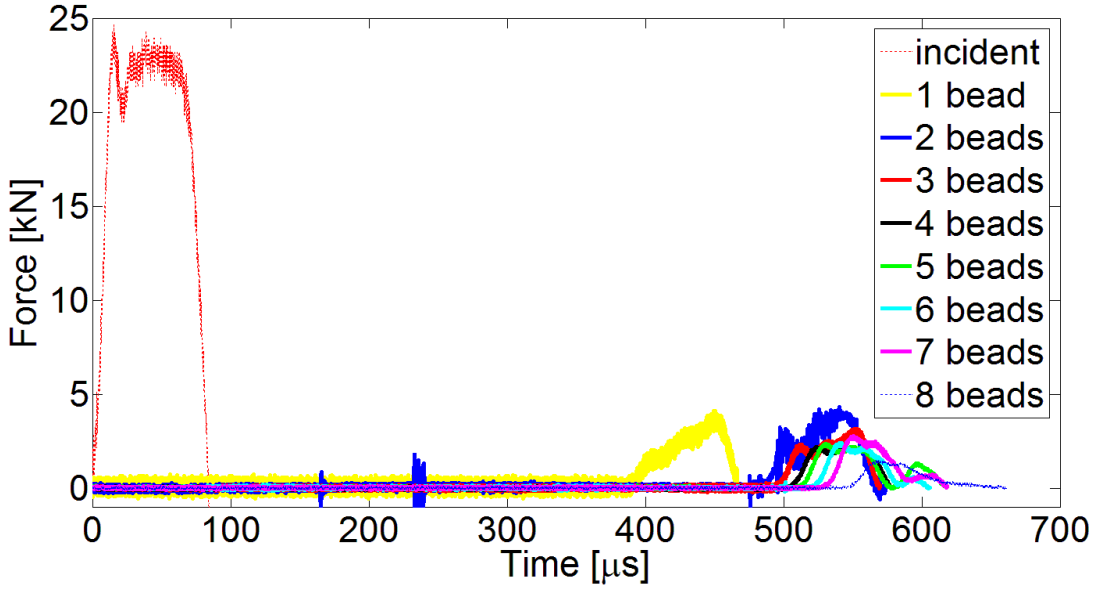

Figure 4.18. Unaltered signal for aluminum beads of various chain lengths.

The calculated plastic solitary wave speed for the aluminum chains as a function of length are shown in Figure 4.19 and are greater than that of brass. However, the dilatational wave speed of aluminum is also greater than the dilatational wave speed of brass. The ratio of dilatational wave speed of aluminum compared to brass is roughly 1.4, whereas the ratio of the plastic solitary wave speed of aluminum compared to brass is approximately 1.6. Similar to the brass plastic wave speed which appears to reach a plateau around six beads, the aluminum wave speed appears to level off around the same length. However, additional tests for the same lengths are needed to determine which data points are consistent and accurate.

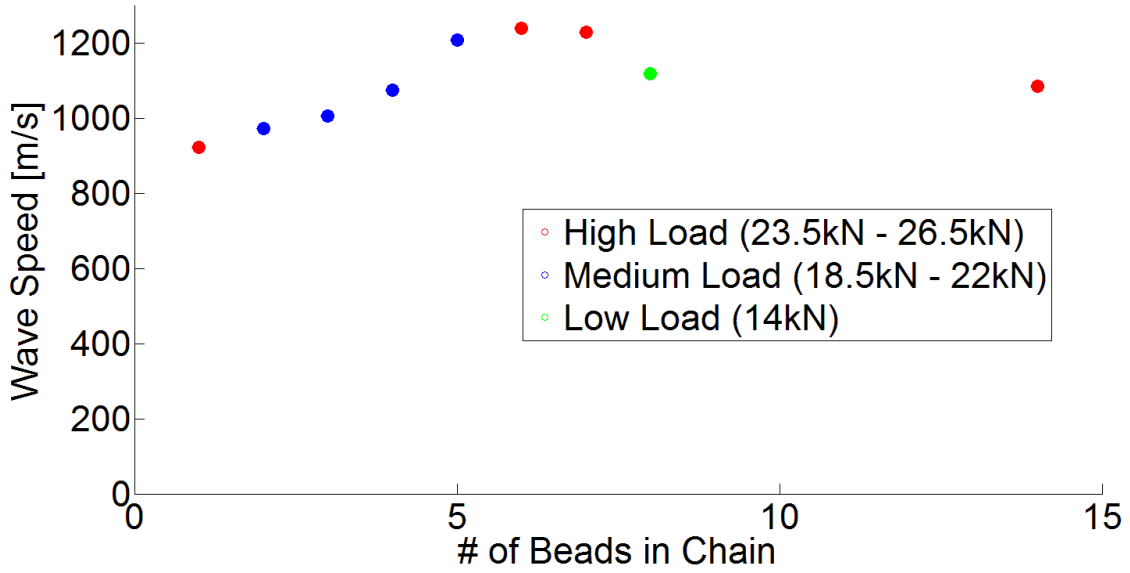

Figure 4.19. Plastic wave speed through one-dimensional aluminum beads of various chain lengths.

The variation of wave speed with both the maximum incident force and the maximum transmitted force is also investigated for the aluminum experiments consisting of five or more beads, and is shown in Figure 4.20 and Figure 4.21 respectively. In this case, however, the power fit for these aluminum wave speeds is closer to the $1/6^{th}$ scaling from one-dimensional elastic granular chain theory, but the number of data points is limited. More experiments are required on the aluminum material, and at higher loads to conclusively answer the wave speed force dependence question.

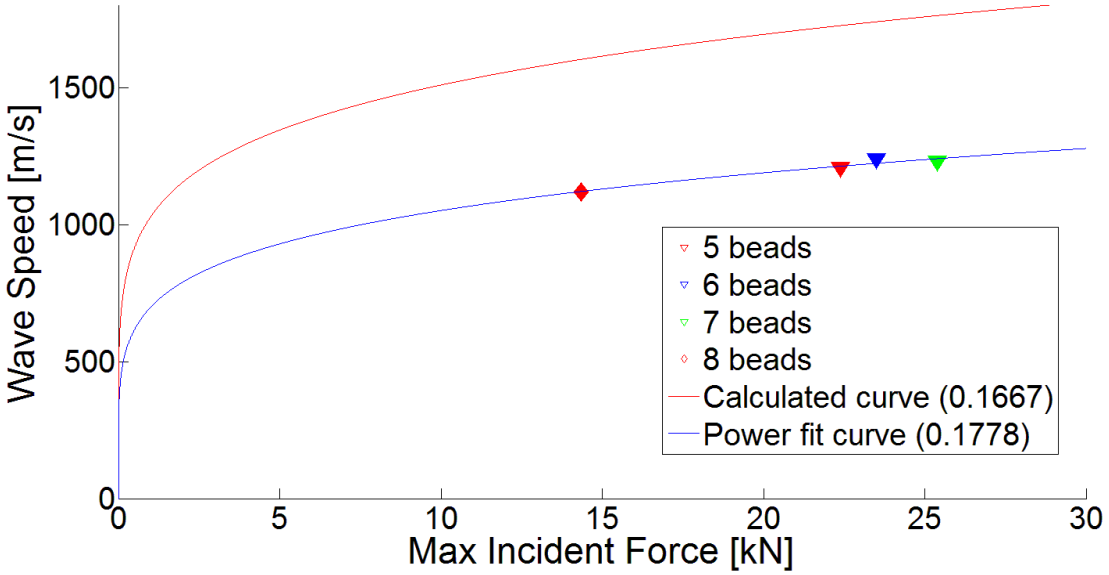

Figure 4.20. Wave speed vs. maximum incident force for various aluminum bead chains.

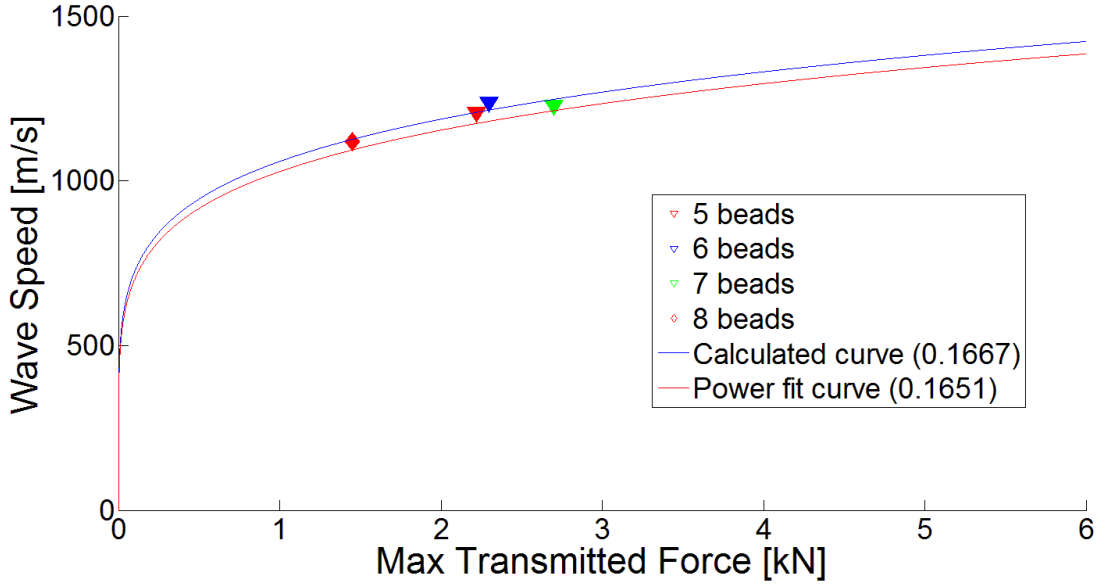

Figure 4.21. Wave speed vs. maximum transmitted force for various aluminum bead chains.

4.2.2 *Stainless Steel (Alloy 302)*

Stainless steel is the last material tested with such one-dimensional homogenous granular chains. Limited testing was conducted on this material because an even larger impact force than

aluminum is needed to produce yielding in this case. Data from the dynamic material response of stainless steel was inconclusive, and the static loading did not reach a large enough load to yield the cylindrical sample, and therefore, was not presented in chapter 3. Regardless, two experimental data sets were acquired and are displayed in Figure 4.22 for chains of thirteen and fourteen steel beads. The longer chain again exhibits a longer time delay for the transmitted wave to propagate. Contrary to both brass and aluminum, however, is the shape of the wave after the primary pulse. Brass displayed a gradual decrease after the peak is reached, while aluminum portrayed in increase peak duration, followed by a rapid unloading of the stress wave. Stainless steel appears to contain both those qualities. The stress wave decreases after the primary peak, similar to brass, but reduces to a second steady stress level instead of dropping to zero. This secondary force level is maintained for a duration which is comparable to the duration of the primary loading and unloading.

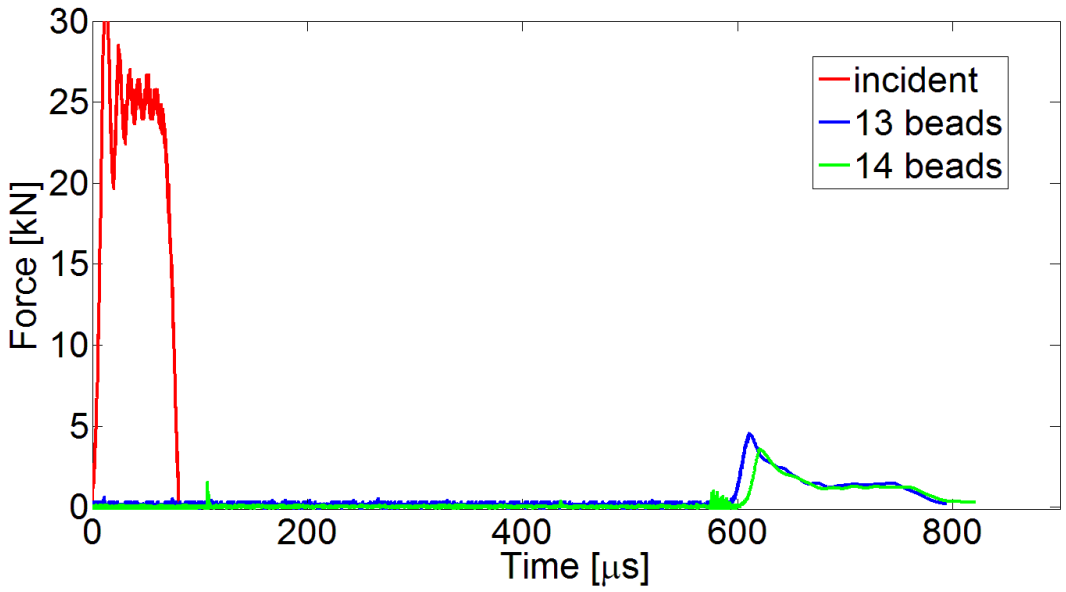

Figure 4.22. Unaltered signal for stainless steel beads of various chain lengths.

Studying the transmitted signals created by brass, aluminum, and stainless steel showed more detail on the evolution of the solitary wave. Comparing the differences and similarities of

the transmitted force as the specimen length increases allows a discrete view on how the solitary wave evolves. The behavior of this transmitted wave is affected by the amplitude of the loading pulse in addition to the material and length the wave propagates through. Such variables can affect the profile of the transmitted stress wave, the wave speed of the chain, and the amount of plasticity the chain undergoes.

Chapter 5

Conclusions

The SHPB was used as a dynamic loading tool to load granular chains beyond the elastic regime in order to study the propagation of solitary waves when plasticity is present. Granular chains of up to fourteen beads were loaded in this fashion. These chains were comprised of brass 260, aluminum 2017, or stainless steel 302. Both brass and aluminum were found to be rate insensitive.

By analyzing the transmitted wave for different chain lengths, and comparing these signals as the chain length increases, a transition in wave behavior was identified. Similar to the elastic case, the critical length for this transition resides between four and five beads, in which the transmitted signal started to behave in a predictable manner. After this critical length, for similar input amplitude and duration, the transmitted wave decayed in amplitude as the chain length increased. Also, the duration of the transmitted wave increased along with the chain length. Each of these propagated signals show signs of a primary pulse, similar to a cos^4 function in shape, followed by a trail of decaying waves of lower amplitude. Prior to reaching this critical length, the transmitted signal varied in signal duration, and showed multiple peaks of a magnitude comparable to the primary pulse.

The speed of the propagating wave within the chain was calculated to be less than its elastic counterpart for the same load. This speed was compared to the elastic relation of $V_{elastic} \propto F_{max}^{1/6}$, and the plastic velocity was found to be $V_{plastic} \propto F_{max}^{1/9}$. The slower plastic velocity is

caused by the nonlinear contact between beads, in addition to dissipative effects from plasticity itself.

The plasticity measurements did not show a monotonic decrease in force for every chain. The shorter chains displayed a varying amount of plasticity while the longer chains had a more consistent decrease. This may be caused by the solitary wave still being formed and is unstable or nonexistent in the shorter chains, while it has become more established in the longer chain. Additional work is needed to explore this issue further.

Regarding future work, additional experiments on different lengths of aluminum and stainless steel chains are needed to further affirm the evolution of the solitary wave in those materials, for which less data was acquired than for brass. Having more data will allow better comparisons and differences in the plastic solitary wave for different materials. This can help identify if and how much of an impact material properties have on this propagating wave. Experimentation on longer aluminum chains is needed to extract a better velocity relation with the maximum force. Having data from tests using a lower force can also benefit the set of brass data, to compare if the $1/9^{th}$ power relation remains consistent. Additional measurements on the physical deformation of different materials can also be used to compare differences between materials. Though less amount of yielding is expected from the stronger material, it can be beneficial to identify whether the varying plasticity occurs independently from material properties, and be a stabilizing effect on the solitary wave.

References

Baker, W.E., Yew, C.H., *Strain-rate effects in the propagation of torsional plastic waves*. J. Appl. Mech. 33, 917-923 (1966).

Bardet, J.P., Vardoulakis, I., *The asymmetry of stress in granular media*. International Journal of Solids and Structures 38, 353-367 (2001).

Bouchaud, J.P., Claudin, P., Levine, D., and Otto, M., *Force chain splitting in granular materials: A mechanism for large-scale pseudo-elastic behaviour*. The European Physical Journal E 4, 451-457 (2001).

Cates, M.E., Wittmer, J.P., Bouchaud, J.P., and Claudin, P, *Jamming, Force Chains, and Fragile Matter*. Phys Review E 31, (1998).

Chang, C.S., Ma, L., *A micromechanical-based micropolar theory for deformation of granular solids*. International Journal of Solids and Structures 28, 67-86 (1991).

Christensen, R.J., Swanson, S.R., Brown, W.S., *Split-Hopkinson-bar tests on rocks under confining pressure*. Exp. Mech. November, 508-513 (1972).

Christoffersen, J., Mehrabadi, M.M., Nemat-Nasser, S., *A Micromechanical description of granular material behavior*. J. Appl. Mech, ASME 48, 339-344 (1981).

Coste, C., Falcon, E., and Fauve, S., *Des Ge´omate´riaux aux Ouvrages*. edited by Petit, C., Pijaudier-Cabot, G., and Reynouards, J.M., Hermes, Paris, (1995).

Coste, B., Falcon, E., and Fauve, S., *Solitary waves in a chain of beads under Hertz contact*. Phys Review E 56, (1997).

Daraio, C., Nesterenko, V.F., Herbold, E.B., and Jin, S., *Tunability of Solitary Wave Properties in One-Dimensional Strongly Nonlinear Phononic Crystals*. Phys Review E 73, (2006).

Davis, J.L., *Wave Propagation in Solids and Fluids*, Springer-Verlag, New York, (1988).

Davis, E.D.H., and Hunter, S.C., *The dynamic compression test of solids by the method of the split Hopkinson pressure bar*. J. Mech. Phys. Solids 11, 155-179 (1963).

Goddard, J.D., Proc. R. Soc. London, Ser. A 430, 105 (1990).

Hertz, H., J. Reine Angewandte Mathematik 92, 156 (1882).

Hopkinson, B., *A method of measuring the pressure produced in the detonation of high explosives or by the impact of bullets*, Philos. Trans. R. Soc. London, Ser. A 213, 437–456 (1914).

Iida, K., Bull. Earthquake Res. Inst. (Tokyo) 16, 131 (1938).

Iida, K., Bull. Earthquake Res. Inst. (Tokyo) 17, 783 (1939).

Johnson, K.L., *Contact Mechanics*. Cambridge University Press, Cambridge, (1985).

Kanatani, K., *A micro-polar continuum theory for the flow of granular materials.* International Journal of Engineering Science 17, 419-432 (1979).

Kolsky, H., *An Investigation of the Mechanical Properties of Materials at very High Rates of Loading,* Proc. Phys. Soc. B, Vol 62, (1949).

Lazaridi, A.N., and Nesterenko, V.F., *Observation of a New Type of Solitary Waves in a One-Dimensional Granular Medium.* J. Appl. Mech. Technol. Phys. (USSR) 26, 405 (1985).

Li, Z., and Lambros, J., *Determination of the dynamic response of brittle composites by the use of the split Hopkinson pressure bar.* Comp. Sci & Tech. 59, 1097 (1999).

Lubliner, J., *Plasticity Theory*. Macmillan, New York (1990).

Nemat-Nasser, S., *Introduction to High Strain Rate Testing.* ASM Vol. 8, Mechanical Testing and Evaluation Handbook, 427-428, (2000).

Nemat-Nasser, S., Isaacs, J.B., Starrett, J.E., *Hopkinson techniques for dynamic recovery experiments*. Pro. Royal Soc. London 435, 371-391 (1991).

Nesterenko, V.F., J. Appl. Mech. Tech. Phys. 24, 733 (1983).

Nesterenko, V.F., J. Appl. Mech. Tech. Phys. (USSR) 5, 733 (1984).

Nesterenko, V.F., *Dynamics of Heterogeneous Materials,* Springer-Verlag, New York, (2001).

Ravichandran, G., and Subhash, G., *Critical Appraisal of Limiting Strain Rates for Compression Testing of Ceramics in a Split Hopkinson Pressure Bar.* J. Amer. Ceram. Soc. 77 (1994).

Sadd, M.H., Qiu, L., Boardman, W.G., and Shukla, A., *Modelling Wave Propagtion in Granular Media Using Elastic Networks.* Int. J. Rock Mech. Min. Sci. & Geomech. Abstr. Vol 29, No. 2, 161-170 (1992).

Sen, S., Hong, J., Bang, J., Avalos, E., and Doney, R., *Solitary waves in the granular chain.* Phys. Rep. 462 (2008).

Shukla, A., *Dynamic Photoelastic Studies of Wave Propagation in Granular Media*. Optics and Lasers in Engineering 14, 165-184, (1991).

Shukla, A., Sadd, M.H., and Mei, H., *Experimental and Computational Modeling of Wave Propagation in Granular Materials.* Exp. Mech. 377-381, (1990).

Shukla, A., Zhu, C.Y., and Xu, Y., *Dynamic stresses in granular assemblies with microstructural defects.* J. Engrg. Mech. 118, 190-201 (1992).

Song, B., Chen, W., Antoun, B.R., Frew, D.J., *Flow stress obtained on ductile specimens deforming at high strain rates*. Exp. Mech. 47, 671-679 (2007).

Wang, E., and Lambros, J., *Experimental investigation of plastic dynamic contact laws*, in preparation, (2011).